Laminar and Subcellular Heterogeneity of GLAST and GLT-1 Immunoreactivity in the Developing Postnatal Mouse Hippocampus

Alexandra E. Schreiner,[1] Simone Durry,[1] Tomomi Aida,[3] Martin C. Stock,[2] Ulrich Rüther,[2] Kohichi Tanaka,[3,4,5] Christine R. Rose,[1]* and Karl W. Kafitz[1]

[1]Institute of Neurobiology, Heinrich Heine University Duesseldorf, 40225 Duesseldorf, Germany
[2]Institute for Animal Developmental and Molecular Biology, Heinrich Heine University Duesseldorf, 40225 Duesseldorf, Germany
[3]Laboratory of Molecular Neuroscience, Medical Research Institute, Tokyo Medical and Dental University, Tokyo, 113-8510, Japan
[4]The Center for Brain Integration Research, Tokyo Medical and Dental University, Tokyo, 113-8510, Japan
[5]Core Research for Evolutional Science and Technology, Japanese Science and Technology Agency, Saitama, 113-8510, Japan

ABSTRACT

Astrocytes express two sodium-coupled transporters, glutamate–aspartate transporter (GLAST) and glutamate transporter-1 (GLT-1), which are essential for the maintenance of low extracellular glutamate levels. We performed a comparative analysis of the laminar and subcellular expression profile of GLAST and GLT-1 in the developing postnatal mouse hippocampus by using immunohistochemistry and western blotting and employing high-resolution fluorescence microscopy. Astrocytes were identified by costaining with glial fibrillary acidic protein (GFAP) or S100β. In CA1, the density of GFAP-positive cells and GFAP expression rose during the first 2 weeks after birth, paralleled by a steady increase in GLAST immunoreactivity and protein content. Upregulation of GLT-1 was completed only at postnatal days (P) P20–25 and was thus delayed by about 10 days. GLAST staining was highest along the stratum pyramidale and was especially prominent in astrocytes at P3–5. GLAST immunoreactivity indicated no preferential localization to a specific cellular compartment. GLT-1 exhibited a laminar expression pattern from P10–15 on, with the highest immunoreactivity in the stratum lacunosum-moleculare. At the cellular level, GLT-1 immunoreactivity did not entirely cover astrocyte somata and exhibited clusters at processes. In neonatal and juvenile animals, discrete clusters of GLT-1 were also detected at perivascular endfeet. From these results, we conclude there is a remarkable subcellular heterogeneity of GLAST and GLT-1 expression in the developing hippocampus. The clustering of GLT-1 at astrocyte endfeet indicates that it might serve a specialized functional role at the blood–brain barrier during formation of the hippocampal network. J. Comp. Neurol. 522:204–224, 2014.

© 2013 Wiley Periodicals, Inc.

INDEXING TERMS: astrocyte; GFAP, S100β; perivascular endfeet; EAAT

Glutamate is the major excitatory neurotransmitter of the central nervous system. Upon its release into the extracellular space, it is efficiently removed by high-affinity, sodium-dependent glutamate transporters, located at neuronal and glial plasma membranes (Rothstein et al., 1994; Danbolt, 2001; Takayasu et al., 2009). Astrocytes, which express the glutamate transporters glutamate-aspartate transporter/excitatory amino acid transporter 1 (GLAST/EAAT1; Storck et al., 1992) and glutamate transporter 1/excitatory amino acid transporter 2 (GLT-1/EAAT2; Pines et al., 1992), account for the majority of the glutamate uptake activity in the brain (Danbolt et al., 1992; Matsugami et al., 2006). Glial glutamate uptake results in a fast decline in the extracellular glutamate concentration, shapes the time course of synaptic conductance, contributes to the input specificity of glutamatergic synapses, and prevents excitotoxicity (Danbolt, 2001). Furthermore, Na^+ signals accompanying glutamate uptake have been

© 2013 Wiley Periodicals, Inc.

Grant sponsor: The Deutsche Forschungsgemeinschaft; Grant number: Ro2327/4-3.

*CORRESPONDENCE TO: Christine R. Rose, Institute of Neurobiology, Heinrich Heine University Duesseldorf, Universitaetsstrasse 1, Building 26.02.00, 40225 Duesseldorf, Germany. E-mail: rose@uni-duesseldorf.de

Received October 11, 2012; Revised May 23, 2013;
Accepted August 2, 2013.
DOI 10.1002/cne.23450
Published online August 12, 2013 in Wiley Online Library (wileyonlinelibrary.com)

proposed to serve a central role in coupling glial to neuronal metabolism (Deitmer and Rose, 2010; Allaman et al., 2011).

In addition to their function at established synapses, glutamate transporters have also been assigned a critical role during development and maturation of neuronal networks (Kudryashov et al., 2001; Nosyreva and Huber, 2005) by regulating neuronal migration (Shibata et al., 1997; Matsugami et al., 2006), proliferation (Gilley and Kernie, 2011), and synapse formation and function (Matsugami et al., 2006). In the hippocampus proper, as in most brain regions, neurogenesis is largely completed at birth, whereas gliogenesis and astrocytic maturation are still in progress and parallel dendritic growth and synaptic maturation (Pfrieger, 2002; Ming and Song, 2005; Freeman, 2010). Astrocyte differentiation comprises reorganization of fine processes and formation of defined cellular domains (Bushong et al., 2004), formation of the gap junctional network (Schools et al., 2006), and alterations in ion channel and transporter expression (Bordey and Sontheimer, 1997; Seifert et al., 2009).

The general expression pattern of astrocytic glutamate transporters has been the focus of several investigations (Danbolt, 2001). Earlier studies employing immunohistochemistry at the ultrastructural level showed that in the rat hippocampus and cerebellum, both GLAST and GLT-1 are located close to synapses and at a lower level at perivascular astrocyte endfeet (Chaudhry et al., 1995; Lehre et al., 1995; Lehre and Danbolt, 1998). Immunohistochemistry at the light microscopic level and immunoblotting further revealed significant differences between different brain regions and established a general increase in glutamate transporter expression from birth to adulthood (e.g., Rothstein et al., 1994; Furuta et al., 1997; Ullensvang et al., 1997). In addition, it was found that GLAST is predominantly expressed by radial glial cells and immature astrocytes, whereas GLT-1 is regarded as the major transporter of mature astrocytes (Hartfuss et al., 2001; Yang et al., 2009).

Because astrocytes are decidedly polarized cells, with delicate perisynaptic processes contacting synapses on one side and highly specialized endfeet contacting blood vessels on the other (Mathiisen et al., 2010; Reichenbach et al., 2010), glutamate transporter expression might be heterogeneous not only in respect to development, but also at the cellular and subcellular level. In the present study, we therefore investigated the laminar and subcellular protein expression profile of GLAST and GLT-1 hippocampus of mice during postnatal development by using immunohistochemistry, western blot analysis, and high-resolution fluorescence microscopy.

MATERIALS AND METHODS

Animals and tissue preparation

All experiments were carried out in accordance with the institutional guidelines of the Heinrich Heine University Duesseldorf as well as the European Communities Council Directive (86/609/EEC). Balb/c mice (*Mus musculus*) of both genders at different postnatal stages (P3–P5; P10–P15; P20–P25; adults [P60–P70]) were used for this study. Animals older than P10 were decapitated following CO_2 anesthesia, which was omitted in younger animals. Brains were quickly removed and immersion-fixed for 2–3 days at 4°C in 4% paraformaldehyde (PFA) in phosphate-buffered saline (PBS; pH 7.4). The tissue was stored in PBS for at least 1 day at 4°C until it was sliced on a Vibratome (Campden Instruments, Leicester, UK).

Experiments carried out on tissue derived from GLAST−/− ($n = 4$) and GLT-1−/− ($n = 6$) animals and the wild-type littermates ($n = 7$ and $n = 4$ respectively; Tanaka et al., 1997; Watase et al., 1998; Matsugami et al., 2006; Aida et al., 2012) were performed in accordance with the ethical guidelines of the Institutional Animal Care and Use Committee of Tokyo Medical and Dental University (0130166C). Tissue was treated as described for the Balb/c mice, and fixed brains were transported in ice-cold PBS. These experiments were carried out as a blind case study.

Transversal hippocampus sections (30 μm) were used for immunohistochemical processing. For stimulated emission depletion (STED) microscopy, slices of P15 animals were prepared on an HM 650 V Vibratome (8 μm, Thermo Scientific, Limburg, Germany).

All chemicals were purchased from Sigma-Aldrich (Munich, Germany) if not stated otherwise.

Antibody characterization

All antibodies employed in this study are listed in Table 1. The following antisera, representing well-established, commercially available standard markers, were utilized in this study: guinea-pig GLT-1 antiserum directed against the C-terminus of rat GLT-1 (Millipore, Tullagreen Carrigtwohill, Ireland; e.g., Benediktsson et al., 2012), guinea pig GLAST antiserum directed against the C-terminus of rat GLAST (Millipore, Ireland; e.g., Zhou et al., 2006), and monoclonal anti-mouse GLAST (ACSA-1; Militenyi Biotech, Bergisch-Gladbach, Germany; Jungblut et al., 2012). In addition to previous studies showing validation of these antibodies (Suaréz et al., 2000; Zhu et al., 2008; Brunne et al., 2010; Jungblut et al., 2012), a detailed characterization of these antibodies is provided by the present study. The specificity of the antibodies was verified by comparing their labeling patterns in −/− animals with that of wild-type littermates (see Results).

TABLE 1.

Primary Antibodies Used in This Study

Antibody	Structure of the immuno-gen	Manufacturer	Order no.	Lot no.	Species	Type	Dilution	Application	Listed
GLAST (EAAT1)	KPYQLIAQDNEPEKPVADSETKM	Chemicon/Millipore	AB1782[1]	LV1395302; JC1615843; JC1658217	Guinea pig IgG	Polyclonal	1:1,000	IHC	Yes
GLAST (EAAT1)	n.s.	Miltenyi Biotec	130-095-822 (ACSA-1)	5120724190	Mouse IgG2a	Monoclonal	1:100	IHC	No
GLAST (EAAT1)	KPYQLIAQDNEPEKPVADSETKM	Tocris Bioscience	2064	1	Rabbit IgG	Polyclonal	1:2,000	WB	No
GLT-1 (EAAT2)	AANGKSADCSVEEEPWKREK	Chemicon/Millipore	AB1783	LV1377592; LV1547805; LV1688372	Guinea pig IgG	Polyclonal	1:1,000/ 1:2,000	IHC/WB	Yes
GFAP	n.s. (full-length protein from cow spinal cord)	Dako Cytomation	Z 0334	00036063	Rabbit IgG	Polyclonal	1:1,000 / 1:2,000	IHC/WB	Yes
GFAP	clone G-A-5(LQSLTCDVESLRGTNESLERQMRE QEERHAREAASYQEALTRLEEEGQSLK DEMARHLQEYQELLNVKLALDIEIATY)	Sigma-Aldrich	G3893	078K4830	Mouse IgG	Monoclonal	1:1,000/ 1:2,000	IHC/WB	Yes
S100β	n.s. (recombinant full-length cow protein)	Abcam	ab868	877135; 200026	Rabbit IgG	Polyclonal	1:100	IHC	No
α-Actin	SGPSIVHRKCF	Sigma-Aldrich	A2066	090M4758	Rabbit IgG	Polyclonal	1:2,000	WB	Yes
α-Tubulin	Clone 6-11B-1	Santa Cruz Biotechnology	sc-23950	B0711	Mouse IgG	Monoclonal	1:2,000	WB	No
GAPDH	Clone 71.1	Sigma-Aldrich	G8795	080M4806	Mouse IgM	Monoclonal	1:20,000	WB	Yes
Mouse IgG	AF488 conjugated	Invitrogen (Life Technologies)	A11029	56881A	Goat	–	1:100	IHC	Yes
Mouse IgG	AF633 conjugated	Invitrogen (Life Technologies)	A21050	690316; 796022	Goat	–	1:100	IHC	No
Rabbit IgG	AF594 conjugated	Invitrogen (Life Technologies)	A11012	47098A; 695244	Goat	–	1:100	IHC	No
Guinea pig IgG	AF488 conjugated	Invitrogen (Life Technologies)	A11073	400881; 629114; 753761	Goat	–	1:100	IHC	Yes
Mouse IgG	HRP conjugated	Dako Cytomation	P0260	00039217	Rabbit	–	1:2,000	WB	No
Rabbit IgG	HRP conjugated	Dako Cytomation	P0448	00041782	Goat	–	1:2,000	WB	No
Guinea pig IgG	HRP conjugated	Sigma-Aldrich	A5545	089K4858	Rabbit	–	1:2,000	WB	No
Rabbit IgG	Cromeo-494 conjugated	Active Motif	15042	1	Goat	–	1:100	IHC	No
–	Atto647N streptavidin conjugated	ATTO-TEC	AD647N-61	1	–	–	1:50	IHC	No
Guinea pig IgG	Biotinylated	Biozol	BA-7000	V0615	Goat	–	1:100	IHC	No

[1]Unfortunately, the manufacturer has lately stopped the sale and distribution of this GLAST antibody.

Abbreviations.GLAST, glutamate aspartate transporter; GLT-1, glutamate transporter 1; GFAP, glial fibrillary acidic protein; AF, Alexa Fluor; GAPDH, glycerinaldehyde-3-phosphate-dehydrogenase; IHC, immunohistochemistry; HRP, horseradish peroxidase; WB, western blot; n.s., not specified.

For specific identification and morphological characterization of astrocytic cells, polyclonal rabbit antibodies against glial fibrillary acidic protein (GFAP; GFAP-pAb; DakoCytomation, Glostrup, Denmark; Wu et al., 2005; Brunne et al., 2010) and S100β (Abcam, Cambridge, UK; Magavi et al., 2012) were employed. As the specific epitope(s) of GFAP-pAb was (were) not determined, we compared the gained staining pattern with results obtained with a monoclonal mouse antibody detecting GFAP (GFAP-mAb) (Sigma Aldrich; Olabarria et al., 2010; Brunne et al., 2010). Control experiments employing double labeling with antibodies for neuronal structures and the antibodies used in the present study never showed colocalization, suggesting that the labeling presented here is of a purely glial nature.

According to the manufacturer, the GFAP-mAb epitope amino acid sequence is: LQSLTCDVESLRGTNESLERQMREQEERHAREAASYQEALTRLEEEGQSLKDEMARHLQEYQELLNVKLALDIEIATY. The database UniProtKnowledgeBase revealed that this sequence corresponds to part of the coil IIb structure of the rod domain. Both GFAP-mAb and GFAP-pAb labeled the same cells and subcellular compartments; however, more structures were visualized by GFAP-pAb. All three antibodies (S100β, GFAP-mAb, and GFAP-pAb) reliably stained cells that could be identified by either prior SR-101 incorporation, which is a vital dye exclusively taken up by astrocytes, or cells expressing green fluorescent protein (GFP) under the GFAP promoter (data not shown). Thus these antibodies can be considered to recognize their supposed target specifically. Moreover, virtually all S100β-positive cells stained positive for GFAP (data not shown).

Standard fluorochrome-conjugated antibodies (Alexa Fluor, Invitrogen, Carlsbad, CA) were used as secondary antibodies for immunohistochemistry. To visualize immunoblots, HPR-conjugated antibodies were used (for details, see Table 1).

Except for ACSA-1, all antibodies used for immunohistochemistry were employed for western blot analysis. To ensure comparability, the investigated specimen was in both cases murine hippocampal tissue. For all antibodies used, the patterns of the bands and their molecular weight were comparable with calculated (e.g., utilizing the ExPASy compute pI/Mw tool) and experimental data published by other groups (e.g., Haugeto et al., 1996; Suaréz et al., 2000; Brunne et al., 2010).

Immunohistochemistry

Hippocampal sections were permeabilized and blocked in PBS containing 0.25% Triton-X-100 (TX) and 2% normal goat serum (NGS, Invitrogen; blocking reagent) for 90 minutes at 4°C followed by incubation with rabbit anti-GFAP (1:1,000) or rabbit anti-S100β (1:100, in blocking reagent) overnight at 4°C. After five washes (2X brief, 3X 15 minutes), sections were incubated either with guinea pig anti-GLAST, with guinea pig anti-GLT-1 (both 1:1,000, 4 hours at room temperature [RT]), or with mouse-anti-GLAST (1:100, 12 hours, 4°C). All the following working steps were likewise performed at RT. Excess primary antibody was removed with five washes (2X short, 3X 15 minutes) using 2% NGS in PBS. Anti-rabbit Alexa Fluor 594 and anti-guinea pig Alexa Fluor 488 were used for visualization of antibody binding (both 1:100, 2% NGS/PBS, 2 hours). Following six washes in PBS (10 minutes each), a 4,6-diamidino-2-phenylindole (DAPI; Invitrogen) counterstain was performed. The slices were washed another three times (10 minutes) and mounted on glass slides with Mowiol/DABCO (Fluka; Calbiochem, San Diego, CA). For super-resolution microscopy, biotinylated anti-guinea pig (1:50, 2% NGS/PBS, 2 hours; Biozol, Eching, Germany) together with streptavidin-conjugated Atto 647N ((1:100, 2% NGS/PBS, 2 hours); Atto Tec, Siegen, Germany) and Chromeo 494 (Active Motif, La Hulpe, Belgium) were employed as secondary antibodies (1:100, 2% NGS/PBS, 2 hours). Labeling patterns were identical to those found with the Alexa fluorophores.

Identical conditions in tissue processing were employed in all individually performed stainings. Negative controls were run in parallel to each staining by omitting either all or one of the primary antibodies. Control stainings omitting one of the primary antibodies exhibited identical labeling patterns for the remaining antibody as for the double stainings. Excluding both primary antibodies never resulted in a labeling product. This was equally true for tissue processed for confocal and for STED microscopy.

Changes in the number of GFAP-immunopositive cells in the hippocampal CA1 subregions (strata oriens, pyramidale, and radiatum) of the different age groups were assessed utilizing maximum projections of whole-frame confocal z-stacks (159.84 × 119.84 μm, 30-μm-thick z-stack, 30 optical sections each 1 μm). Independent measurements were performed for each age cohort. Densities of GFAP(+) cell bodies were calculated per volume tissue, on the basis of the field of analysis and the thickness of the tissue probe imaged. All GFAP(+) cell bodies depicted in a given frame were treated as a count. Data for the experimental groups were expressed as the mean number of cells ± standard error of the mean (SEM).

Western blotting

For western blotting, whole hippocampi or the hippocampal CA1 subfield including the strata oriens,

pyramidale, and radiatum were excised, frozen in liquid nitrogen, and homogenized at 4°C in radioimmunoprecipitation assay (RIPA) buffer containing 1% deoxycholic acid (NP-40), 0.25% sodium deoxycholate, protease inhibitors (CompleteMini, Roche, Mannheim, Germany), 150 mM NaCl, and 50 mM Tris-HCl adjusted to a pH of 7.4. The homogenate was centrifuged at 13,000g for 10 minutes, and 4X Laemmli sample buffer (5% sodium dodecyl sulfate [SDS], 43.5% glycerol, 100 mM DL-dithiothreitol [DTT], 0.02% bromphenol blue, 20% 2-mercaptoethanol, 125 mM Tris-HCl adjusted to a pH of 6.8) was added to the supernatant. Proteins were electrophoretically separated on 10% gels by SDS-polyacrylamide gel electrophoresis (PAGE). Subsequently, the proteins were transferred electrophoretically to polyvinylidene fluoride (PVDF) membranes. Strips of the PVDF membranes were preincubated in PBS containing 0.1% Tween and 5% milk powder overnight at 4°C. To this blocking solution, either guinea pig anti-GLAST, guinea pig anti-GLT-1, or rabbit anti-GFAP were added at a 1:2,000 dilution and applied to the PVDF membrane for 1 hour (RT). Bound immunoglobulins were visualized by using horseradish peroxidase-conjugated goat anti-rabbit or goat anti-guinea pig IgG at a 1:2,000 dilution (incubated for 30 minutes at RT) and the enhanced luminol chemiluminescence technique (ECL kit, Amersham, Freiburg, Germany). In parallel, detection of the relative protein content of every probe was performed using an antibody against α-actin. The resulting chemiluminescence was detected by using the luminescent image analyzer LAS-4000 (Fujifilm Europe, Dusseldorf, Germany).

For standardization of the probes, an α-actin alignment was performed. Because many proteins change in their expression quantity during postnatal development, leading to incorrect standardization, we additionally performed a glyceraldehydes 3-phosphate dehydrogenase (GAPDH) and α-tubulin alignment of the α-actin alignment. This control experiment demonstrated no difference between α-actin and the housekeeping protein GAPDH, but did show an increase in α-tubulin protein levels. These results are in line with findings showing that expression of the α1 and α2 isoform remains constant during the postnatal period, whereas other α-tubulin isoforms exhibit an increase in protein levels during development. Thus, pan-detection of α-tubulin was not suitable for normalization of protein content of different age stages during the first postnatal weeks, and α-actin was used instead in this study.

Western blot data were quantified by using AxioVision software (Zeiss, Göottingen, Germany). Background-corrected gray values of the given protein were divided by the α-actin gray value. All resulting data were normalized to the value determined for the adult animals.

Confocal and STED microscopy and image processing

Immunofluorescence was analyzed by a confocal laser scanning system on an Olympus BX51WI microscope (FV300, Olympus, Hamburg, Germany). Images were collected with either a 20×/0.50 (UMPlanFI, Olympus), a 40×/0.80 (LUMPlan, Olympus) water immersion or a 60×/1.40 (PlanApoVC, Nikon, Duesseldorf, Germany) oil immersion objective. A Kalman filter 4 was applied for every scan. Fluorescent images labeled with Alexa Fluor 488 and Alexa Fluor 594 were collected by using excitation wavelengths of 488 nm (multiline argon ion laser) and 543 nm, respectively (helium neon laser; both Melles Griot, Bensheim, Germany). Simultaneous or sequential scanning of both fluorophores revealed no difference in their staining pattern, indicating no cross-excitation or spectral bleed-through. Stacks of optical sections (1 μm) were taken. Extended focus images are shown as indicated in the figure legends and were calculated from z-stacks of optical sections by using ImageJ software (NIH, Bethesda, MD). Images were overlaid employing Adobe Photoshop CS2 (Adobe Systems, San Jose, CA). The PMT settings and the image processing were kept constant when the different age groups were compared.

To improve spatial resolution, documentation of sets ($n = 5$) of immunofluorescence-labeled tissue slices was further performed by taking advantage of super-resolution microscopy employing a TCS SP5 STED microscope (Leica Instruments, Mannheim, Germany) with a 100× /1.4 NA STED oil objective (Leica Instruments). Fluorophores were excited by pulsed lasers (excitation wavelengths: 531 nm and 635 nm; Pico Quant, Berlin, Germany). Depletion was achieved by using a MaiTai HP BB laser (SpectraPhysics, Darmstadt, Germany) at 750 nm. Every image underwent 2D deconvolution using LASAF software (Leica Instruments). Color coding and slight adjustments in brightness of the final figures were done with Adobe Photoshop CS2. For adjustments in brightness, all images were corrected with the identical settings.

Statistics

Unless specified otherwise, data are expressed as means ± SEM. Data were analyzed using an unpaired Student's *t*-test. In all cases, a P value < 0.05 expressed a significant difference ($*P < 0.05$; $**P < 0.01$; $***P < 0.001$). "*n*" represents the number of slices and "*N*" the number of individuals, if not stated

otherwise. Origin 8.5 software (OriginLab, Friedrichsdorf, Germany) was employed for statistical evaluation.

RESULTS

GFAP expression in the developing hippocampal CA1 region

For identification of astrocytes, we used GFAP, a well-characterized and widely used marker for mature astrocytes including at least a subset of radial glial cells (Brunne et al., 2010; Middeldorp and Hol, 2011). We first established the time course of GFAP expression as well as the number of GFAP-positive cells during postnatal development in our preparation by immunohistochemistry and western blot analysis. To this end, we employed a polyclonal antibody against GFAP, which exhibited favorable properties compared with a monoclonal antibody tested for this study. Preliminary tests revealed that GFAP-pAb binds to more astrocytic structures, particularly in neonate astrocytes and radial glial cells, and that extra protein bands are detected in western blots, the molecular weight of which matches well the specific GFAP isoforms (not shown; Middeldorp and Hol, 2011). Thus, we employed GFAP-pAb for our study as an astrocytic pan-marker, as proposed earlier (Brunne et al., 2010).

Labeling the hippocampal CA1 region for GFAP revealed considerable changes in the density and distribution of GFAP-immunoreactive structures during postnatal development (Fig. 1A–C). From P3–P5 ($n = 24$; $N = 11$) to P10–P15 ($n = 28$; $N = 14$), the density of GFAP-immunoreactive structures exhibiting astroglial morphology increased especially within the strata oriens and radiatum. Afterward, these parameters remained stable until adulthood. Morphological analysis at the cellular level revealed that the structure, which was labeled by GFAP immunoreactivity, changed its intracellular organization during the first postnatal weeks (Fig. 1D–G). In general, the GFAP immunoreactivity in the neonate hippocampus at P3–P5 appeared frayed and rough (Fig. 1D). Later on, the GFAP-immunoreactive structures became more and more evenly shaped and homogenously distributed (Fig. 1E–G) pointing to a rearrangement and modification of the intracellular GFAP network.

Cell counting in the CA1 region of the hippocampus revealed that the number of GFAP-immunoreactive cells per μm^3 tripled from P3–P5 to P10–15 (3.3 $\pm$ 0.2 and 10.8 $\pm$ 0.4 GFAP-positive cells per 100,000 μm^3, respectively; Fig. 1H). Thereafter, a stable value of approximately 7 GFAP-positive cells per 100,000 μm^3 was found for the juvenile and adult (7.8 $\pm$ 0.3 and 7.4 $\pm$ 0.3 per 100,000 μm^3; P20–P25: $n = 29$; $N = 14$; adult: $n = 28$; $N = 4$). In aged animals (18 months), this value was maintained (6.7 $\pm$ 0.2 per 100,000 μm^3; $n = 24$; $N = 3$. In summary, our results show a strong increase in the density of GFAP(+) astrocytes in the first and second postnatal week. Between P10–P15 and P20–P25, cell density declined again, probably due to increasing tissue volume during this period.

To quantitatively determine the relative GFAP expression levels, we performed a western blot analysis of the hippocampal CA1 subregion including the strata oriens, pyramidale, radiatum, and lacunosum-moleculare. The 50-kDa GFAP protein content detected in the CA1 homogenates increased abruptly between P3–P5 and P10–P15 (3.1-fold; $P < 0.01$) and remained constant thereafter (P20–P25 and adult tissue; Fig. 1I,J).

Taken together, our results confirm that overall GFAP expression, number, and morphology of GFAP-immunoreactive cells in the hippocampal CA1 region undergo substantial changes during postnatal development.

Verification of anti-GLAST and anti-GLT-1 specificity

To verify the specificity of the antibodies against the transporters GLAST and GLT-1, the GLAST$-/-$ animals (Watase et al., 1998 Matsugami et al., 2006) were immunohistochemically labeled for GLAST, and GLT-1$-/-$ mice (Tanaka et al., 1997; Aida et al., 2012) were labeled for GLT-1 versus their wild-type littermates. Labeling for GLAST in hippocampal tissue derived from GLAST$-/-$ animals resulted in no or barely detectable products for the transporter (Fig. 2A–F). The same was true for the immunohistochemical staining products when anti-GLT-1 was employed in GLT-1$-/-$ mice. Virtually no GLT-1 signal could be detected in the GLT-1$-/-$ animals (Fig. 2G–L).

Generally, the signals revealed for the transporters in the $-/-$ animals corresponded to what was found in the negative control labels (data not shown). In the wild-type littermates, in contrast, high-intensity signal levels were obtained for both GLAST and GLT-1 antibodies. In the wild types, labeling signals for both glial transporters were always associated with glial structures, as revealed by counterstaining for GFAP (Fig. 2). Neuronal somata did not exhibit detectable staining products of the antibodies employed for the glia-specific transporters. Labeling patterns of the two different antibodies used for immunohistochemical labeling for GLAST, guinea pig anti-GLAST, and mouse anti-GLAST (ACSA-1), matched closely (data not shown).

These results strongly suggest that labeling for both GLAST and GLT-1 was highly specific in the hippocampal region of murine tissue.

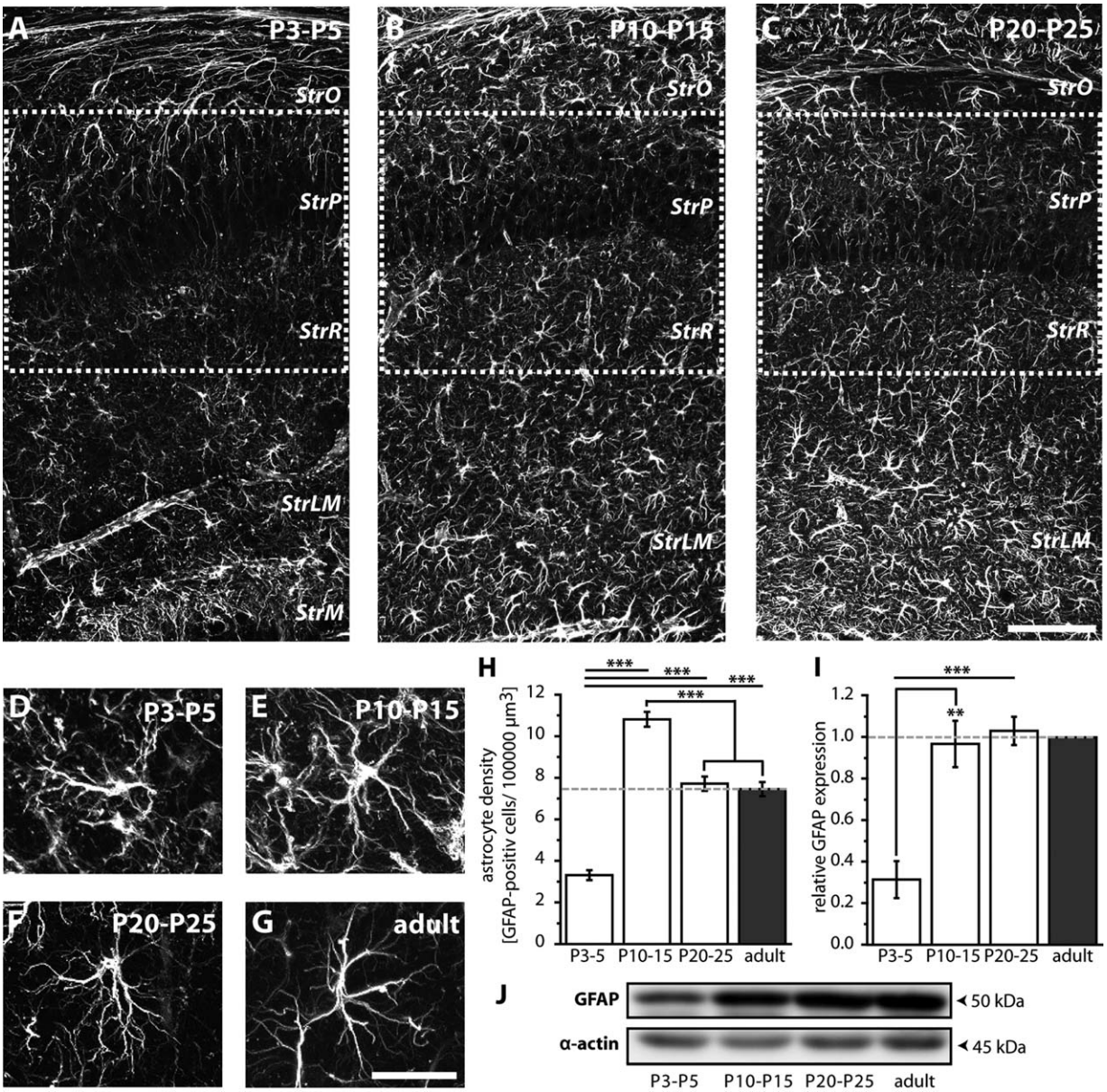

Figure 1. GFAP expression during postnatal development. Immunohistochemical labeling for GFAP of transverse sections of the mouse hippocampus at the indicated developmental stage. **A–C:** GFAP staining of the hippocampal CA1 subregion. Overviews of the CA1 area representing extended focus images from z-stacks of 15 serial z-sections of 1 µm. The boxes delineate the areas in which GFAP-positive astrocytes were counted (see H). **D–G:** Morphology of GFAP-positive astrocytes at the indicated developmental stages. **H:** Histogram showing the number of GFAP-positive cells (astrocytes) per 100,000 μm^3 in the CA1 region. Cells were counted in one image section through the depth of the slice, corresponding to 30 µm (P3–P5: $n = 22$, $N = 11$; P10–P15: $n = 28$, $N = 14$; P20–P25: $n = 35$, $N = 15$; adults (P60–P70): $n = 24$, $N = 4$). **I, J:** Canonic GFAP expression in CA1 homogenates: (J) representative western blot and (I) western blot-based analysis of relative GFAP expression at indicated developmental stages ($N = 3$ for each age group). Shown are mean values ± SEM; $***P < 0.001$; $** P < 0.01$; $* P < 0.05$. StrO, stratum oriens; StrP, stratum pyramidale; StrR, stratum radiatum; StrLM, stratum lacunosum-moleculare, StrM, stratum moleculare. Scale bar = 20 µm in A (applies to A–C); 50 µm in G (applies to D–G).

Distribution of GLAST immunoreactivity in CA1

Having verified the specificity of the antibodies for GLAST and GLT-1, we performed double staining to detect either GLAST or GLT-1 together with GFAP in neonate (P3–P5; both: $n = 12$ and $N = 11$), early postnatal (P10–P15; both: $n = 14$; $N = 14$), juvenile (P20–P25; GLAST: $n = 15$; GLT-1: $n = 14$; both: $N = 14$), and adult mice (P60–P70; GLAST: $n = 13$; GLT-1: $n = 15$; both: $N = 4$) to visualize astroglial glutamate transporter expression. In the neonate hippocampus (P3–P5), prominent GLAST immunoreactivity was observed

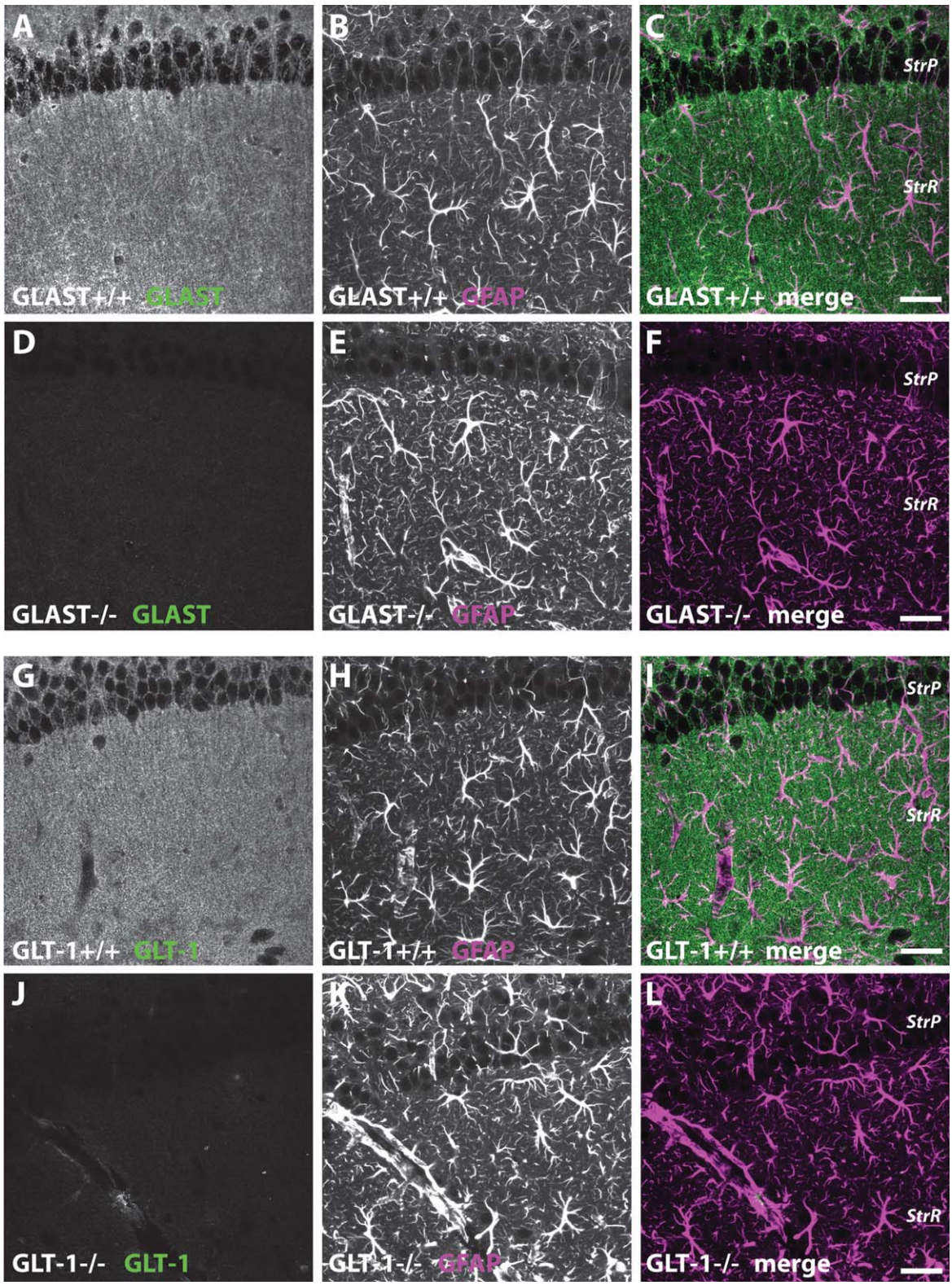

Figure 2. Verification of the specificity of the GLAST and GLT-1 labeling. Images represent maximum projections of five consecutive optical CLSM sections (1 μm) of the hippocampal CA1 region of P22. **A–F:** GLAST-/- mice (D–F) and their wild-type littermates (A–C) immunohistochemically labeled for GLAST (left panel) and GFAP (middle panel) and the merge (right panel). **G–L:** GLT-1-/- mice (J–L) and their wild-type littermates (G–I) immunohistochemically labeled for GLT-1 (left panel) and GFAP (middle panel) and the merge (right panel). StrP, stratum pyramidale; StrR, stratum radiatum. Scale bar = 20 μm in C (applies to A–C), F (applies to D–F), I (applies to G–I), and L (applies to J–L).

in the CA1 region, particularly along radially elongated GFAP-positive processes that traverse the strata oriens and pyramidale. GLAST-immunoreactive cells without GFAP labeling were only found in exceptional cases (Fig. 3A–C). In the stratum radiatum, mainly astrocytic cell bodies were labeled for GLAST (cf. Fig. 6). Both the GFAP as well as the GLAST labeling pattern in this layer exhibited a narrow stellate morphology.

At P10–P15, some of the astrocytes traversing the pyramidal cell layer showed an intense immunoreactivity like the unipolar radial processes observed in the neonate (Fig. 3D–F). Compared with earlier developmental stages, these cells showed a more branched morphology. At P10–P15, a characteristic labeling along fine fibers (approximately 0.5 μm in diameter) crossing almost the entire hippocampal subregion appeared for the first time in the strata radiatum and oriens (Fig. 3D–F). The strongest GLAST immunofluorescence was still observed in the stratum pyramidale. Additional punctate GLAST-positive labeling of variable intensities and densities was found in close association with neuronal somata during all stages investigated.

The P20–P25 and adult hippocampi showed quite similar labeling patterns for GLAST (Fig. 3G–L). In the adult, however, fewer astrocytic processes were distinctively labeled by GLAST, and a more homogenous subcellular GLAST distribution was detected. Furthermore, GLAST-immunoreactive puncta, arranged like beads on a chain, passed through the stratum radiatum perpendicular to the pyramidal cell layer in hippocampi from adult animals.

Distribution of GLT-1 immunoreactivity in CA1

In contrast to GLAST (cf. Fig. 3), GLT-1 showed no differential laminar label at P3–P5 (Fig. 4A–C). Only a few detached GLT-1-immunoreactive cells located either in the strata oriens or lacunosum-moleculare were detectable. In these cells, GLT-1 was highly accumulated adjacent to presumptive astrocytic cell bodies (Fig. 4A–C). At P10–15, the GLT-1 immunoreactivity increased significantly, with the weakest protein levels detected throughout the stratum pyramidale (Fig. 4D–F). Almost all GFAP-positive cells showed immunoreactivity for GLT-1 that was especially arranged at the proximal, primary processes and dispersed toward the distal processes.

At P20–P25, GLT-1 was distributed over a larger surface of a given astrocyte and strongly colocalized with GFAP (Fig. 4G–I). In contrast to the inhomogeneous staining pattern of GLT-1 seen during the first 3 weeks of postnatal development, a rather uniform protein distribution was seen in the adult mouse CA1 (Fig. 4J–L). All hippocampal subregions except the stratum pyramidale exhibited similar high expression levels. This homogenous staining pattern might result from the high density of transporter label at GFAP-negative peripheral astrocytic processes.

In conclusion, immunohistochemistry indicated a laminar distribution profile of GLAST and GLT-1 that is established during postnatal development. Immunoreactivity for both glutamate transporters was present in a basically complementary fashion, with GLAST localized predominantly in the stratum pyramidale and predominant GLT-1 localization in other regions of the hippocampus, exhibiting lower levels in the stratum pyramidale. Furthermore, both GLAST and GLT-1 immunoreactivity increased during postnatal development, although GLT-1 exhibited a delayed rise in labeling compared with GLAST.

Developmental changes in GLAST and GLT-1 protein levels

To quantify the relative overall expression levels of both GLAST and GLT-1 in the CA1 region during postnatal development, we performed western blots (Fig. 5). In CA1 homogenates, several bands were detected for both transporters (Fig. 5A,B) that most likely correspond to monomeric and multimeric entities of the transporters, known to exist as homomultimers (Haugeto et al., 1996; Peacey et al., 2009). Numerical summation of the intensity of the different bands revealed that the overall GLAST protein content doubled from P3–P5 to P10–P15 (37.6–70.3% of adult protein content; Fig. 5C). GLT-1 content was very low at P3–P5 and only reached sizable levels at P10–P15 (35.1% of adult protein content). The protein content more than doubled until P20–P25 (76.2% of adult protein content; Fig. 5C).

In summary, we found that both GLAST and GLT-1 protein content increased during the first 2–3 weeks of postnatal development in the CA1 region of the mouse hippocampus, indicating a differential temporal upregulation during postnatal development.

Subcellular expression pattern of GLAST and GLT-1

High spatial resolution analysis of immunostaining was performed to address the subcellular distribution of the two glutamate transporter subtypes. To this end, costaining with S100β, a glial-specific cytosolic calcium binding protein (Raponi et al., 2007), was carried out to better delineate the morphology of the astrocytic cell bodies and processes. Furthermore, maximum intensity

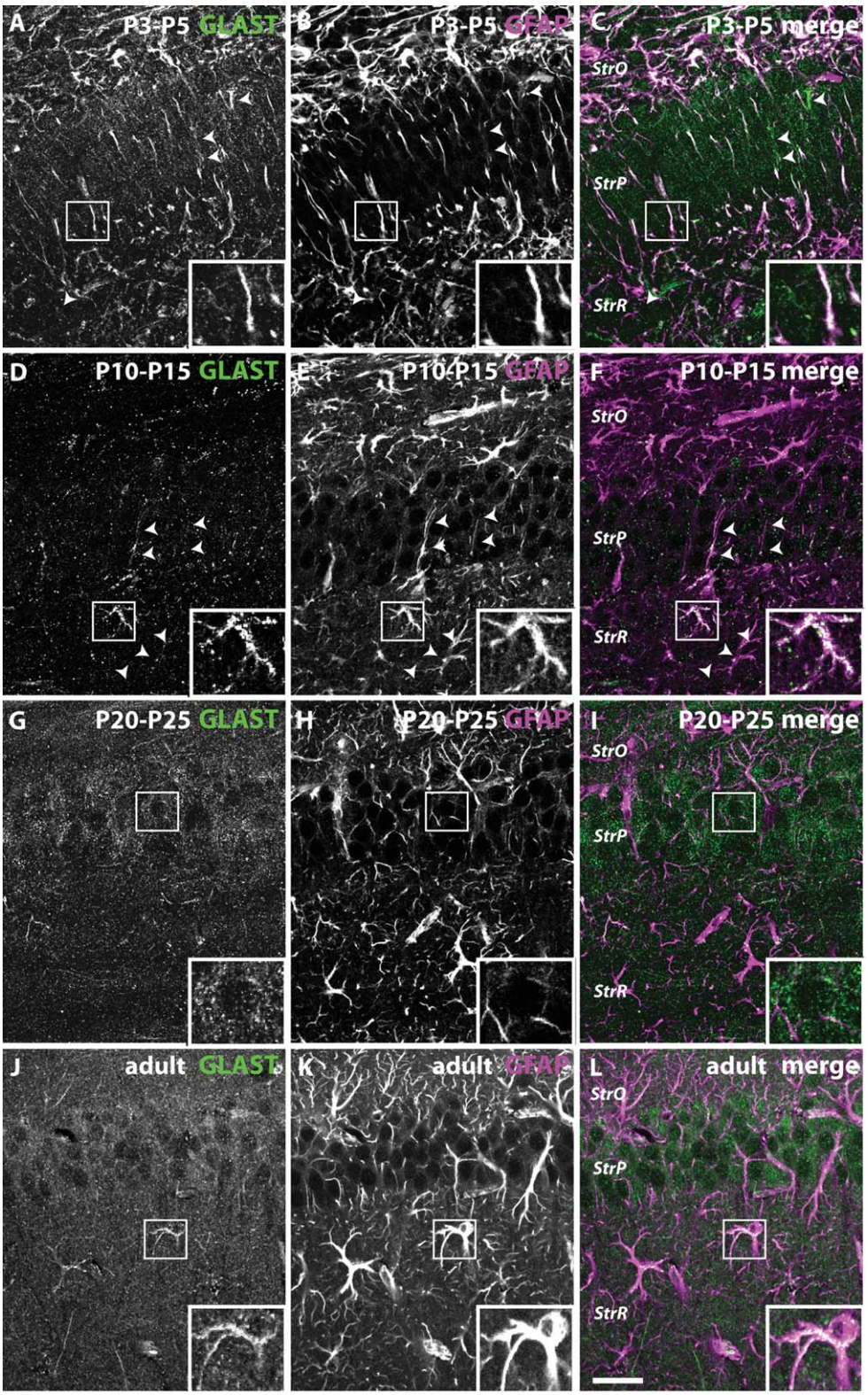

Figure 3. GLAST expression in CA1. Images derived from single optical slices of 1 μm of the hippocampal CA1 region at the indicated developmental stages, immunohistochemically labeled with antibodies directed against GLAST (A,D,G,J) and GFAP (B,E,H,K). C, F, I, and L show the overlay of both channels. **A–C:** In the neonate mouse, robust GLAST immunoreactivity is found in elongated GFAP-positive astrocytic processes traversing the strata oriens and pyramidale. The arrowhead indicates the rare case of a GLAST-positive, but GFAP-negative process. **D–F:** At P10–15, a punctate GLAST labeling pattern around neuronal cell bodies in the stratum pyramidale is established. Robust GLAST expression was found in more branched cells at this developmental stage. Arrowheads point to a thin (~0.5 μm) structure labeled for GLAST that crosses several astrocytic domains. **G–L:** At P20–25 (G–I) and in adult mice (J–L), a laminar distribution is established with highest GLAST expression around neurons of the pyramidal cell layer. Al, alveus; StrO, stratum oriens; StrP, stratum pyramidale; StrR, stratum radiatum. Scale bar = 20 μm in L (applies to A–L).

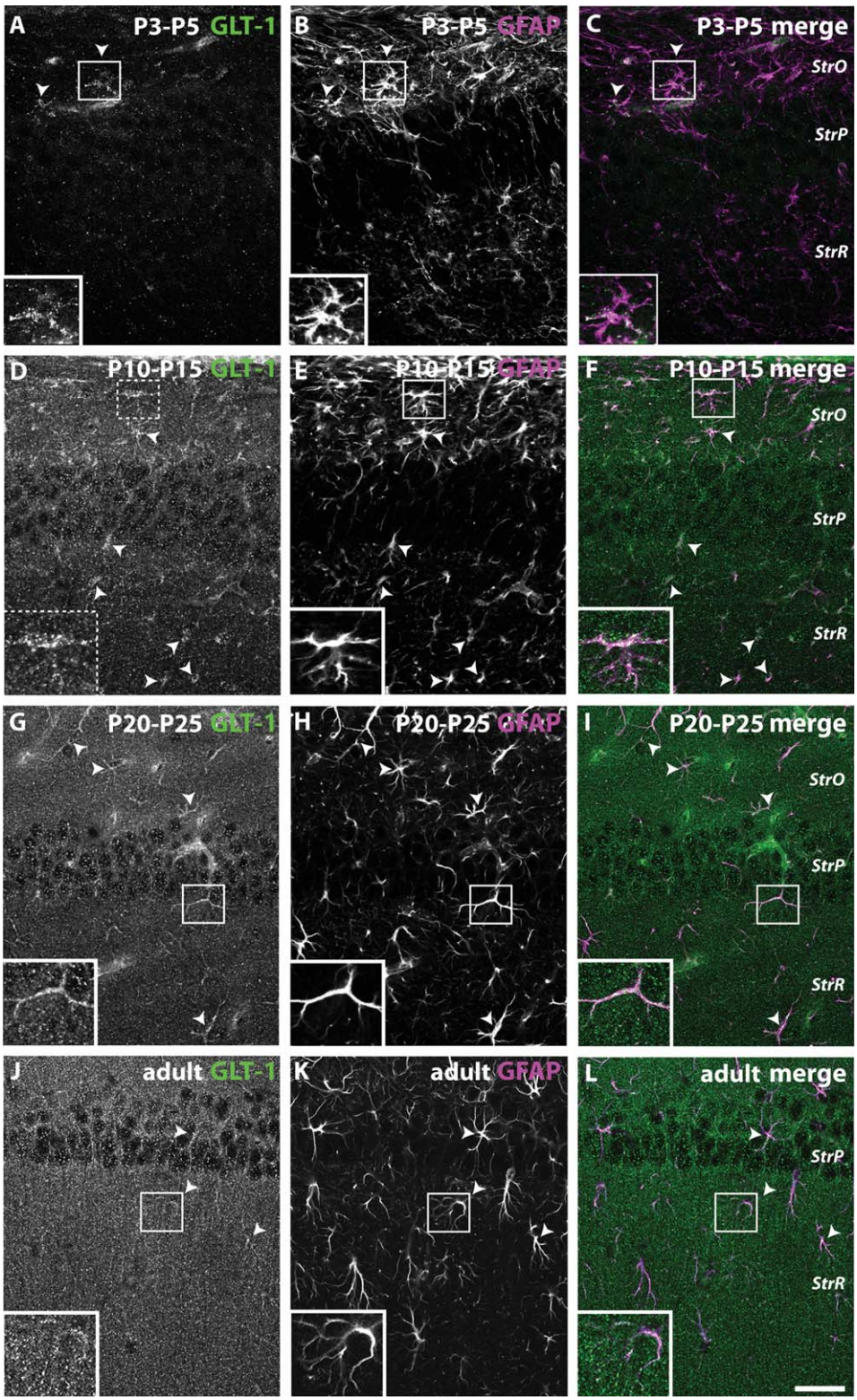

Figure 4. GLT-1 expression in CA1. Images derived from single optical slices of 1 μm of the hippocampal CA1 region at the indicated developmental stages, immunohistochemically labeled with antibodies directed against GLT-1 (A D,G,J) and GFAP (B,E,H,K). C, F, I, and L show the overlay of both channels. **A–C:** In the neonate, only a few GLT-1 positive cells are detectable in the strata oriens and radiatum. **D–F:** GLT-1 protein levels as well as the number of distinctly labeled cells increase by P10–P15. **G-I:** At P20–25, GLT-1 highly colocalizes with GFAP. **J–L:** GLT-1 labeling in the adult. Arrowheads indicate GLT-1- as well as GFAP-positive astrocytes. Al, alveus; StrO, stratum oriens; StrP, stratum pyramidale; StrR, stratum radiatum. Scale bar = 20 μm in L (applies to A–L)

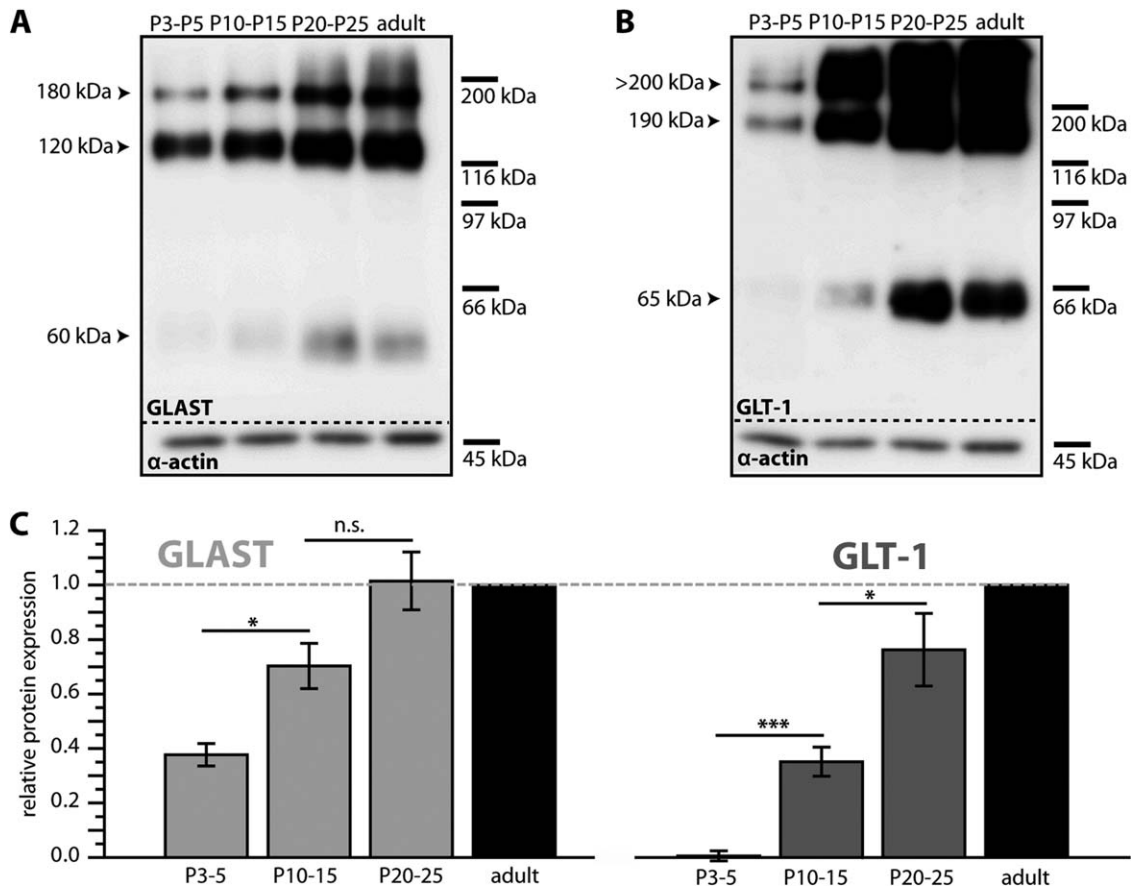

Figure 5. GLAST and GLT-1 protein content in CA1. Western blots of CA1 homogenates developed against GLAST (**A**) and GLT-1 (**B**). **C:** Quantification of total protein content, determined by the numeric summation of the individual bands, for GLAST and GLT-1, respectively. Shown are mean values ± SEM (three animals in each age cohort).

projections derived from stacks of images taken at different depths were generated to enable better visualization of transporter distribution along entire cells. These double stainings showed a rather homogeneous GLAST immunoreactivity at astrocyte somata as well as on processes (Fig. 6A–F). GLT-1 immunoreactivity, in contrast, was predominantly detected on processes, with only sparse labeling of the cell body (Fig. 6G–L).

To further investigate the subcellular distribution of GLT-1 immunoreactivity in astrocytes, we employed super-resolution microscopy using dual-color STED imaging (Willig et al., 2006; Meyer et al., 2008), providing a spatial resolution of less than 50 nm for fluorescent beads (not shown). Dual-color STED imaging resolved clusters of GLT-1 immunofluorescence that were closely associated with filament structures of GFAP (Fig. 7). The direct comparison with images taken in the conventional confocal mode of the laser scanning system (Fig. 7) furthermore revealed that STED microscopy resolved GLT-1 clusters as well as GFAP structures that were not detected with confocal imaging.

Immunohistochemical analysis of astrocyte endfeet on blood vessels indicated another, rather unexpected heterogeneity in the subcellular staining pattern of the two transporter subtypes. Already at P3–P5, a time period when GLT-1 expression was generally very low (cf. Figs. (4 and 5)), pronounced GLT-1 protein clusters were detectable at perivascular endfeet (Fig. 8C,D). At both P10–P15 (Fig. 8M,N) and P25 (Fig. 8G,H), labeling of distinct and dense clusters of GLT-1 was observed on most endfeet. Due to the general increase in GLT-1 in the surrounding neuropil, this pattern was less obvious in tissue derived from adult mice (Fig. 8K,L). In contrast, GLAST was never found to show a comparable concentration of immunoreactive clusters on astrocytic endfeet (Fig. 8A,B,E,F,I,J).

In general, clusters of GLT-1 immunoreactivity on astrocyte endfeet seemed to preferentially colocalize with GFAP (Fig. 8M,N). A close spatial inter-relationship between GLT-1 clusters and GFAP on perivascular endfeet was confirmed by using STED microscopy (Fig. 9). Again, STED microscopy enabled resolution of

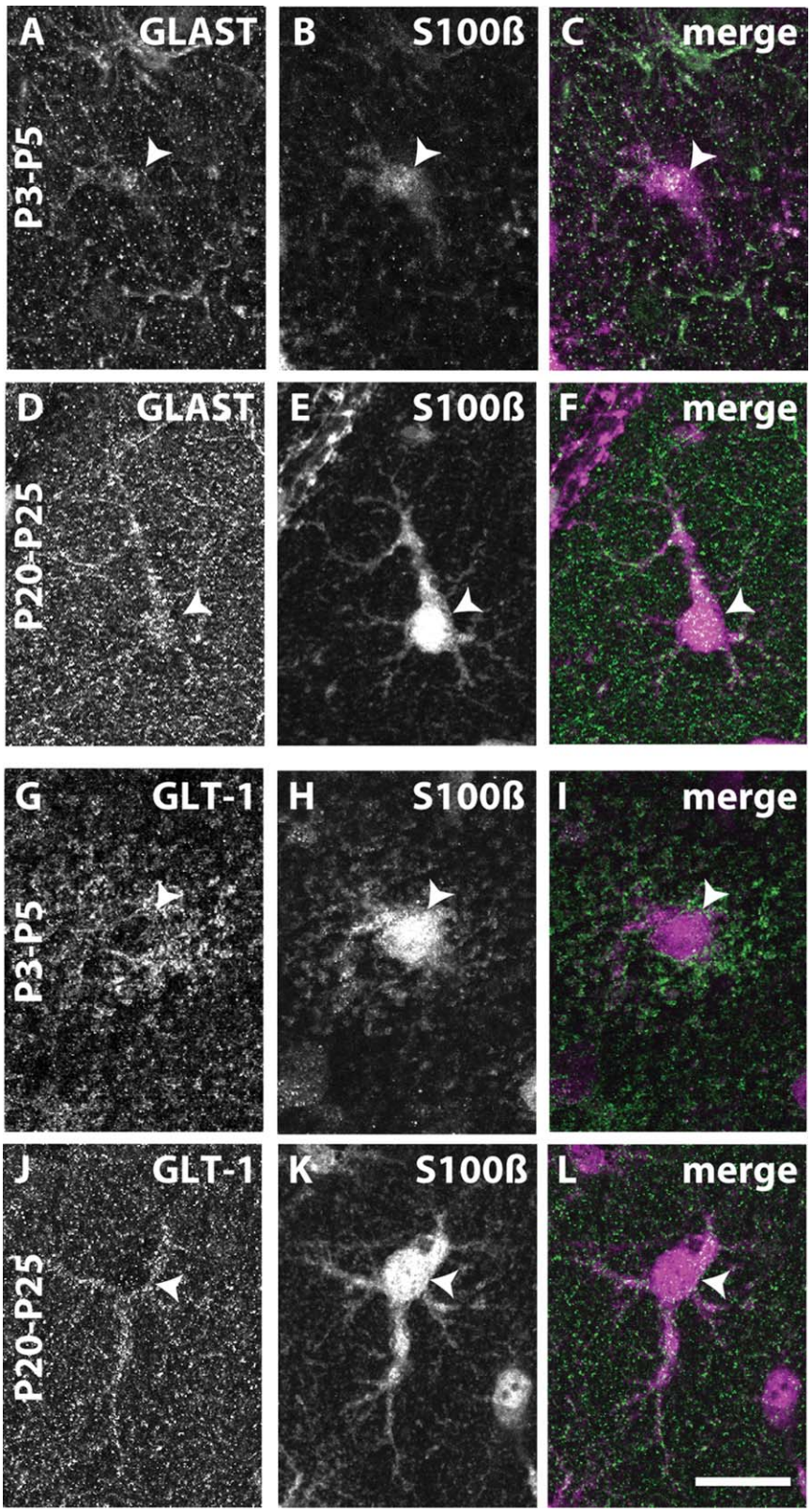

Figure 6. Cellular distribution of GLAST and GLT-1 in CA1. Maximum intensity projections of 10 consecutive optical sections of astrocytes at P3–P5 (A–C; G–I) and P20–P25 (D–F; J–L) labeled with GLAST (**A–F**) or GLT-1 (**G–L**) (Alexa Fluor 488–coupled, left column), and with S100β (Alexa Fluor 594–coupled, middle column). The right column represents the overlay of the two channels. The arrows point to the cell body, which is densely labeled with GLAST (A–F), but virtually avoid of GLT-1 (G–L). Scale bar = 20 μm in L (applies to A–L).

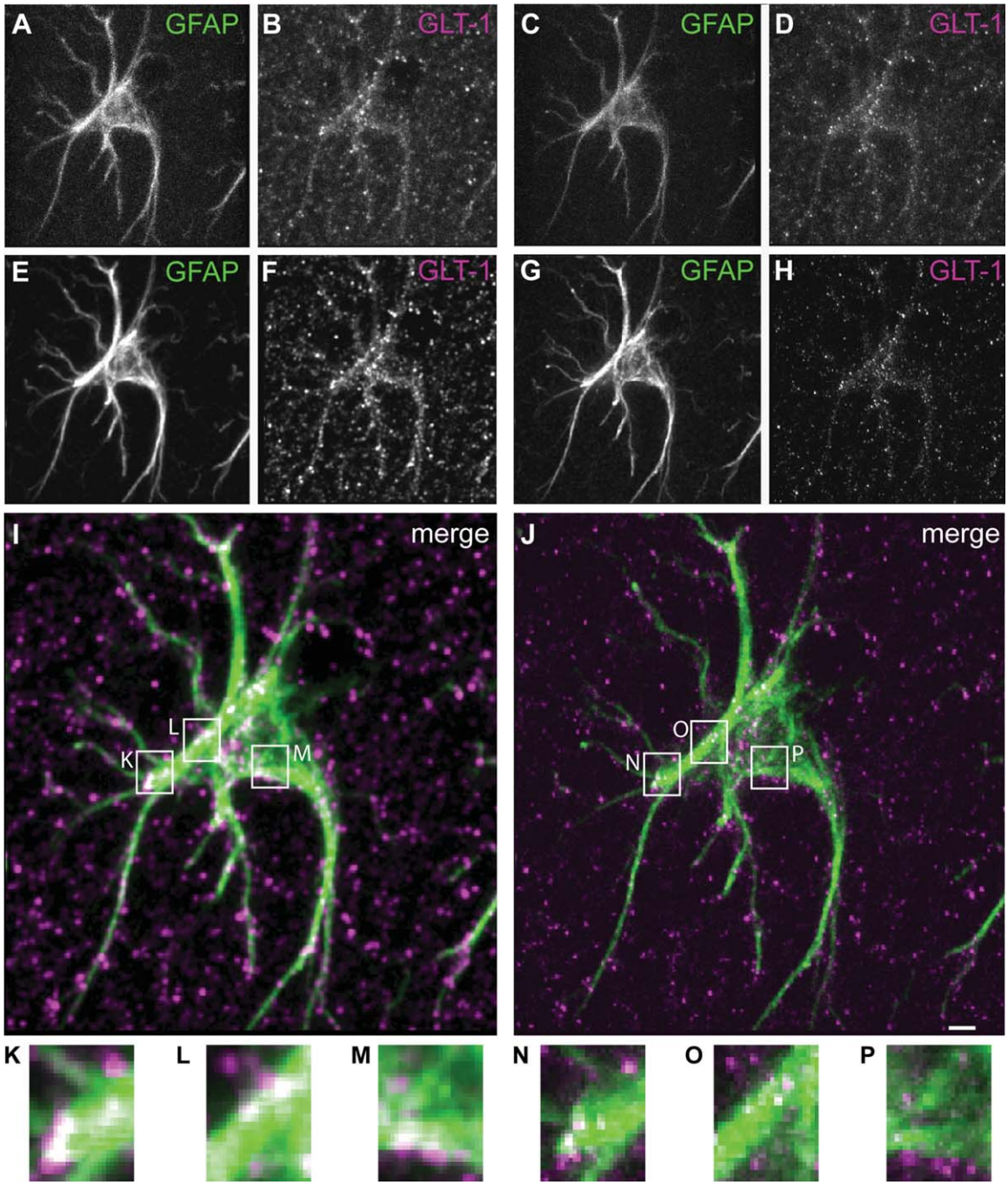

Figure 7. Localization of GLT-1 at a GFAP-labeled astrocyte. **A–P:** Confocal (A,B,E,F,I,K,L,M) and super-resolution images (C,D,G,H,J,N,O,P) of a GFAP-positive astrocyte (Chromeo 494, green) in the stratum radiatum of the mouse hippocampus at P15 and the subcellular localization of the labeling for the glial glutamate transporter GLT-1 (Atto 647N, magenta). The images to the left are taken at a conventional CLSM (Leica SP5). Images taken at the STED microscope are presented to the right. All images except for those presented in the first row (raw images) were processed for xy-deconvolution and postproductionally handled absolutely identically. Note the drastically increased resolution (<50 nm) in the images taken at the STED microscope compared with the images taken at the CLSM. All images represent a maximum projection of 12 optical sections. Scale bar = 2.5 μm in J (applies to A–J).

single clusters of GLT-1 that were not visible in the confocal mode.

In summary, our data suggest a differential expression pattern of the two glutamate transporters on the cellular level and throughout the postnatal development of the hippocampus. Although GLAST immunoreactivity showed no preferential localization to a specific cellular compartment, GLT-1 was particularly found in fine

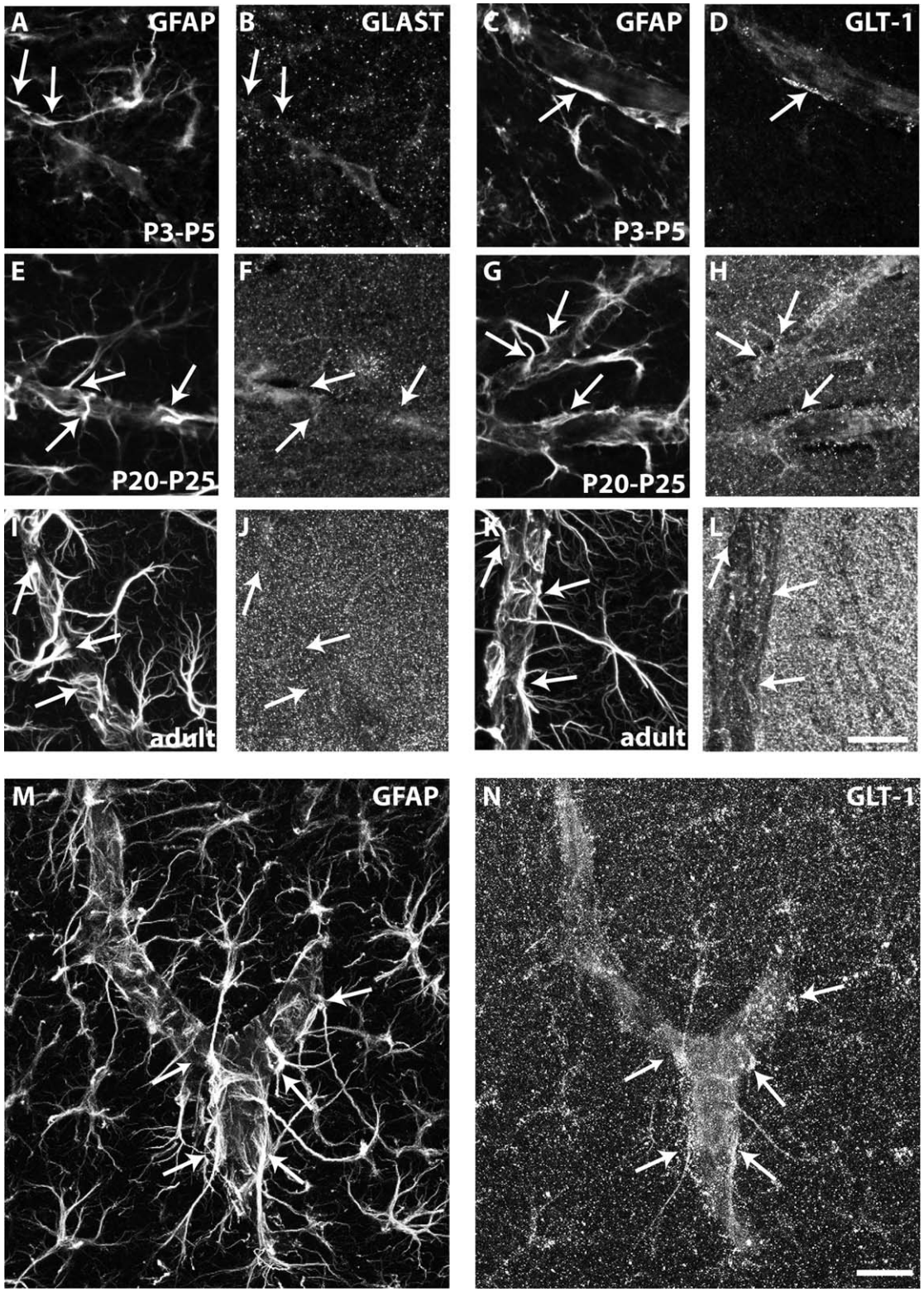

Figure 8. GLAST and GLT-1 labeling pattern at perivascular endfeet. Image of the immunohistochemical staining for GLAST (B,F,J) or GLT-1 (D,H,L,N; both visualized with Alexa Fluor 488), colabeled with GFAP (A,E,I; C,G,K; M; visualized with Alexa Fluor 594), in the stratum radiatum during postnatal development. **A,B,E,F,I,J:** GLAST was not localized on astrocytic endfeet. **C,D,G,H,K,L:** Already at the P3–P5 time period, GLT-1 expression in general was very low; GLT-1 protein clusters were detectable at scattered perivascular endfeet. Between P10 and P25, a pronounced labeling of perivascular endfeet was observed that disappeared in the adult. **M,N:** GLT-1 labeling of a P15 hippocampus. Arrows point to astrocytic endfeet identified by GFAP. Scale bar = 20 μm in L (applies to A–L) and N (applies to M,N).

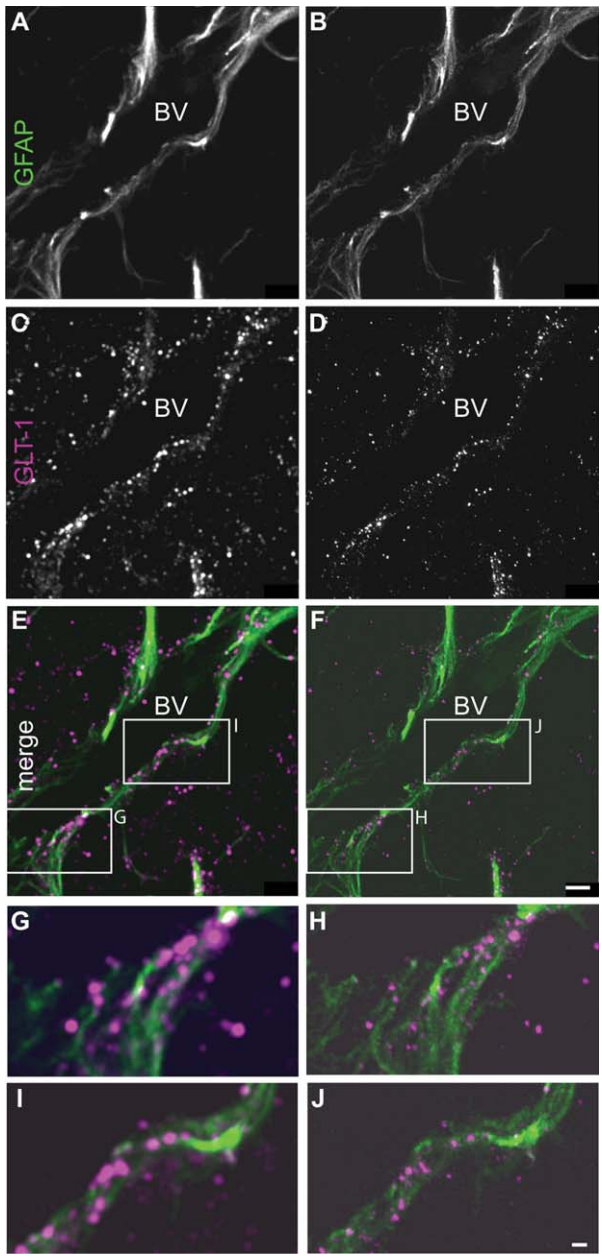

Figure 9. Clusters of GLT-1 at GFAP-labeled astrocyte endfeet. **A–J:** Lining of a blood vessel (BV) in the mouse hippocampus at P15 by GFAP-positive astroglial processes (Chromeo 494, green) and the localization of the labeling for the glial glutamate transporter GLT-1 (Atto 647N, magenta). The images in the left column (A,C,E,G,I) are taken at a conventional CLSM (Leica SP5). Super-resolution images taken at a STED microscope are presented in the right column (B,D,F,H,J). All images were processed for xy-deconvolution and postproductionally handled absolutely identically. All images represent a maximum projection of 10 optical sections. Scale bar = 2.5 µm in F (applies to A–F); 50 nm in J (applies to G–J).

astrocytes processes, with only sparse labeling of the cell bodies. In juvenile animals, distinct GLT-1 clusters were detected at perivascular endfeet, and these clusters seem to preferentially colocalize with GFAP.

DISCUSSION

Our study shows that the density of GFAP-positive cells and GFAP expression increased during the first 2 weeks after birth in the CA1 area of the mouse hippocampus, paralleled by an increase in overall GLAST expression. In addition, our data show that GLAST immunoreactivity increased steadily, with the highest transporter density in neuronal cell body layers and indicate that GLAST was preferentially expressed in astrocytes at P3–P5 and by radial glia. GLAST immunoreactivity was distributed rather homogenously, with no preferential localization to a specific cellular compartment. GLT-1 immunoreactivity was especially prominent in adult tissue. Starting at P10–P15, GLT-1 exhibited a laminar expression pattern, with the highest immunoreactivity in the stratum lacunosum-moleculare. GLT-1 was only sparsely located at astrocyte somata, whereas discrete clusters of immunofluorescence were present at fine processes and at endfeet on blood vessels, where they seemed to preferentially colocalize with GFAP.

Postnatal changes in the levels and cellular organization of GFAP

GFAP, the principal intermediate filament in mature astrocytes, is widely used as a marker to identify cells of the astroglial lineage including radial glial (Shibata et al., 1997; Liu et al., 2006; Raponi et al., 2007). We found a strong increase in the density of GFAP-positive cells from P3–P5 to P10–P15 in the CA1 area, followed by a reduction in cell density to a stable value from P20–P25 on. The observed initial increase in the number of GFAP-expressing cells as well as the decline after P10–P15 are in agreement with earlier results (Nixdorf-Bergweiler et al., 1994; Kimoto et al., 2009). These data are also in line with reports showing that GFAP transcript levels increase until P15 after which they decline again (Riol et al., 1992).

At the cellular level, the GFAP network resembles a rough, fibrous mesh extending from the cell body that is progressively straightened during maturation and limited to the proximal processes (Nixdorf-Bergweiler et al., 1994). Because, under certain conditions, bundles of GFAP filaments can dissociate and expose more epitopes, leading to an artificial increase in antibody-coupled fluorescence, we performed western blots to quantify changes in protein levels. These demonstrate that canonic GFAP increases within the first 2 weeks of postnatal development, confirming results reported earlier (Kim et al., 2011).

GFAP not only controls astrocytic motility and shape by providing structural stability (Rodnight et al., 1997),

but also serves as a scaffold to anchor proteins at the plasma membrane (Middeldorp and Hol, 2011). Indeed, Sullivan and coworkers (2007a) showed that GFAP serves as a cytoskeleton anchor for GLAST. GFAP−/− mice exhibit a reduction in glutamate transport activity, a decrease in GLAST protein expression, and compromised trafficking of GLT-1 to the plasma membrane (Hughes et al., 2004). In addition, GLAST expression and its functionality are prerequisites for proper function of glutamine synthetase and of transmitter clearance in Müller cells of the retina (Derouiche and Rauen, 1995; Ishikawa et al., 2011). In astrocytes, it has been demonstrated that decreasing GFAP levels are accompanied by a rise in glutamine synthetase activity and vice versa (Weir and Thomas, 1984; Lieth et al., 1998; Pekny et al., 1999). These findings strongly indicate that changes in the expression and structural organization of GFAP during postnatal development will also affect the trafficking of glutamate transporters to the plasma membrane and the functionality of the glutamate–glutamine cycle.

Temporal changes in protein content of GLAST and GLT-1

For analysis of temporal changes in the protein levels of GLAST and GLT-1, we employed western blots using two antibodies against GLAST and GLT-1. The anti-GLAST antibody (AB1782) was raised against a synthetic peptide (KPYQLIAQDNEPEKPVADSETKM) corresponding to the carboxy-terminus of rat glutamate transporter GLAST. It does not discriminate between GLAST-1a and GLAST-1b (Vallejo-Illarramendi et al., 2005), two splice variants of GLAST (Lee and Pow, 2010). The anti-GLT-1 antibody was raised against a synthetic peptide (AANGKSADCSVEEEPWKREK) corresponding to the carboxy-terminus of rat glutamate transporter GLT-1.

Our study suggests that the temporal profile of the overall postnatal upregulation of the two glutamate transporters differs: whereas total GLAST had already reached adult protein levels at P10–P15, GLT-1 protein content rose until P20–P25. This differs from results obtained for other regions in the rat brain (i.e., cerebellum, striatum, cortex, and spinal cord), where GLAST expression was basically unaltered from P5 to P16, whereas GLT-1 expression increased steadily (Furuta et al., 1997). The increase in total GLAST protein levels in the mouse CA1 region thus essentially seems to parallel the rise in GFAP protein, whereas GLT-1 protein expression does not necessarily closely follow upregulation of GFAP levels. Our study thus suggests that protein upregulation of glutamate transporters seems to be independently regulated during development. The physiological relevance of such differential regulation is unclear.

Developmental profile of GLAST and GLT-1 immunoreactivity

Analysis of immunohistochemical staining using confocal microscopy confirmed the results obtained by western blot and indicated that GLAST and GLT-1 exhibit changes in their expression pattern during postnatal development of the hippocampus. Although our antibody staining in the GLAST−/− as well as the GLT-1−/− animals has unequivocally shown the specificity of the antibodies used here, it is important to keep in mind that immunocytochemistry does not "show" the proteins directly, but provides, at best, indirect evidence for their presence in the cell of interest (Fritschy, 2008). Even so, the observed overall increase in the labeling intensity for both transporters is in line with earlier studies (Furuta et al., 1997; Kugler and Schleyer, 2004). The results of our staining also support the view that GLAST is the predominant glutamate transporter early in postnatal development and in immature astrocytes and radial glial cells (Shibata et al., 1997; Raponi et al., 2007).

Our data, moreover, also indicate that GLAST expression is not restricted to immature and radial glial cells, but that during maturation virtually all astrocytes upregulate GLAST to moderate levels (Furuta et al., 1997). As mentioned before, the AB1782 antibody employed here was directed against a motif of the antigenic binding site that is found in both isoforms, GLAST1a and GLAST1b. GLAST1b, unlike the astrocyte-specific GLAST1a isoform, is found to be especially located in neuronal cell bodies (Sullivan et al., 2007b). It is still under debate whether GLAST1b represents a functional isoform (Vallejo-Illarramendi et al., 2005).

GLT-1 immunoreactivity increased most discernably between P3–P5 and P10–P15, which also matches the prominent increase in its protein content determined by western blots. The strong increase in GLT-1 protein content and immunolabeling during the first 3 weeks of postnatal development parallels the phase of major synaptogenesis and synapse maturation in the hippocampus (Ullian et al., 2004). Such a coincidental progression has already been described for other brain regions by Furuta and co-workers (1997). Indeed, glutamate uptake through GLT-1 is an important functional element of mature hippocampal synapses (Arnth-Jensen et al., 2002; Verbich et al., 2012), and it was recently shown that GLT-1 protein upregulation during postnatal development is correlated to the frequency of transmitter release at excitatory synaptic sites (Benediktsson et al., 2012).

Subcellular profile of GLAST and GLT-1 immunoreactivity

Immunoreactivity also indicated that specific differences in the subcellular distribution of GLAST and GLT-1 during postnatal development might exist. When evaluating these stainings, it is important to keep in mind that because of the limited spatial resolution of light microscopy, the exact cellular localization of the antigens requires further work. An electron microscopy study providing 3D reconstructions of single astrocytes based on serial sections of immunogold labeling could solve this issue and would thus be highly desirable. In maximum projections, GLAST labeling was specifically found on cell bodies of S100β-positive astrocytes, as well as on their processes. In contrast to GLT-1, GLAST immunoreactivity was rather homogeneously distributed, and we never observed a specific clustering on GFAP-positive endfeet. Thus, even though GFAP has been proposed to enhance glutamate uptake activity and to serve as a cytoskeleton anchor for GLAST (Sullivan et al., 2007a), our data indicate that GLAST might not generally be colocalized with GFAP nor specifically targeted to a subcellular compartment.

Although there is strong evidence for the presence of GLT-1 in axon terminals, it is predominantly expressed by glial cells (Danbolt, 2001; Beart and O'Shea, 2007; Furness et al., 2008; Arranz et al., 2008; Omarani et al., 2009). Earlier work has also established that whereas the majority of transporters are located at the plasma membrane, a significant proportion (~25%) of the protein can be found in intracellular fractions (Nakagawa et al., 2008). Interestingly, the cell surface expression and trafficking of different glutamate transporter isoforms seems to show significant heterogeneity (Beart and O'Shea, 2007).

Similar to GLAST, we found a dot-like, punctate labeling pattern of GLT-1 immunoreactivity on astrocyte processes, a labeling pattern already shown and described by numerous other reports (Zhou and Sutherland, 2004; Nakagawa et al., 2008; Takasaki et al., 2008; Benediktsson et al., 2012). Our maximum intensity projections indicate that GLT-1 might not be homogeneously distributed throughout all cellular domains of astrocytes. They indicate explicit immunolabeling of processes with only sparse labeling of the cell body, the latter preferentially along GFAP-positive fibers.

GLT-1 expression is highly dependent on and sensitive to fast excitatory synaptic transmission (Schlag et al., 1998; Bergles et al., 2002; Nakagawa et al., 2008; Seifert et al., 2009). On the other hand side, GLT-1 is vital for synapse establishment (Benediktsson et al., 2012; Verbich et al., 2012). The close interrelationship and the functional importance of this transporter for synaptic function is also evident from its prominent perisynaptic localization, which has been established by several groups using both electron microscopy and light microscopic techniques (e.g., Chaudry et al., 1995; Minelli et al., 2001; Cholet et al., 2002; Benediktsson et al., 2012). Earlier work has found evidence that sodium signals, which arise following Na^+-dependent glutamate uptake in astrocyte processes (Langer and Rose, 2009), might be a critical modulator in the formation of clusters of GLT-1 at synapses (Nakagawa et al., 2008). Interestingly, perisynaptic astroglial processes are devoid of GFAP, but are characterized by restricted localization of the actin-binding protein ezrin (Derouiche et al., 2002). The interrelationship between ezrin and glutamate transporters, has, to our knowledge, not been studied so far.

Unexpectedly, our staining also indicated a distinct clustering of GLT-1 on GFAP-positive perivascular endfeet during the first 3 weeks of development, but not in adult tissue. In contrast to GLT-1, GLAST immunoreactivity was present, but was never found to show comparable clustering on astrocytic endfeet. The clustering and apparent localization of GLT-1 on endfeet was not only evident with conventional confocal microscopy, but was also seen in super-resolution microscopy, which provided a spatial resolution of 50 nm. Here, GLT-1 clusters were found to be largely overlapping with immunofluorescence for GFAP, indicating that they were indeed located on astrocyte endfeet. Again, because of the limited spatial resolution of immunocytochemistry, our study can only provide an indication, but not ultimate proof of this interesting subcellular localization. Still, earlier work using electron microscopy has already described the presence of GLT-1 as well as GLAST at astrocyte endfeet in the rat brain (Chaudhry et al., 1995; Lehre et al., 1995; Lehre and Danbolt, 1998). Although our findings obtained with immunocytochemistry generally confirm this finding, no explicit differences in the subcellular distribution of GLT-1 and GLAST were reported in these earlier studies. Furthermore, it was found that the astrocyte membranes facing capillaries were less immunoreactive than membranes facing the neuropil (Chaudhry et al., 1995). This apparent discrepancy may be due to the different animal model used (rats as compared with mice). Moreover, whereas no information about the age of the animals was given in the aforementioned papers, it may simply be brought about by the explicit developmental profile found in our study and the fact that the strong clustering of GLT-1 is most visible early in postnatal development.

The possible functional role of clusters of GLT-1 at astrocyte endfeet and the blood–brain barrier already at

a time point where GLT-1 expression is generally very low and no such clusters are seen in the neuropil, is unclear. A recent study on cocultures of endothelial cells and astrocytes provided evidence for an active transport of glutamate in the abluminal-to-luminal direction (Helms et al., 2012). The possible existence of a glutamate "siphoning" mechanism from the brain to the blood is also indicated by studies showing that glutamate entry into the brain is either very slow or virtually not present (Hawkins et al., 1995; Vina et al., 1997). Such a pathway would help to clear the brain tissue from glutamate and might serve a protective role by preventing excitotoxicity. On the other hand, specific clustering of GLT-1 on endfeet could also promote uptake of glutamate and enable rapid detoxification of blood-derived ammonia, which freely diffuses over the blood–brain barrier, in the glutamate/glutamine cycle (Allaman et al., 2011). Indeed, earlier studies demonstrated that a substantial part of the ammonia/ammonium circulating in brain blood vessels passes the blood–brain barrier and becomes incorporated into glutamine through astroglial glutamine synthetase (Cooper et al., 1979; Cooper and Lai, 1987). Glial glutamate transporters on perivascular endfeet might thus serve either one of these processes, glutamate siphoning or ammonia detoxification, depending on the electrochemical driving forces and resulting direction of glutamate transport (Danbolt, 2001).

ACKNOWLEDGMENTS

We thank O. Levai (Leica Instruments, Mannheim, Germany) for providing access to and expert help with the STED system.

CONFLICT OF INTEREST STATEMENT

The authors declare that there is no known or potential conflict of interest including any financial, personal, or other relationships.

ROLE OF AUTHORS

All authors had full access to all the data in the study and take responsibility for the integrity of the data and the accuracy of the data analysis. A.E. Schreiner: immunohistochemistry and western blot experiments, data analysis and interpretation, experimental design, and writing of a first manuscript version. S. Durry: immunohistochemistry and manuscript approval. T. Aida: tissue preparation, genotyping of transgenic animals, and manuscript approval. M.C. Stock: western blot experiments and manuscript approval. U. Rüther: western blot analysis and manuscript approval. K. Tanaka: tissue preparation and genotyping of transgenic animals and manuscript approval. C.R. Rose: project initiation and experimental design, data interpretation, and manuscript writing. K.W. Kafitz: documentation of immunohistochemistry, project design, experimental design, STED microscopy, data interpretation, and manuscript writing

LITERATURE CITED

Aida T, Ito Y, Takahashi YK, Tanaka K. 2012. Overstimulation of NMDA receptors impairs early brain development in vivo. PLoS ONE 7:e36853.

Allaman I, Belanger M, Magistretti PJ. 2011. Astrocyte-neuron metabolic relationships: for better and for worse. Trends Neurosci 34:76–87.

Arnth-Jensen N, Jabaudon D, Scanziani M. 2002. Cooperation between independent hippocampal synapses is controlled by glutamate uptake. Nat Neurosci 5:325–331.

Arranz AM, Hussein A, Alix JJ, Přez-Cerdá F, Allcock N, Matute C, Fern R. 2008. Functional glutamate transport in rodent optic nerve axons and glia. Glia 56:1353–1367.

Beart PM, O'Shea RD. 2007. Transporters for L-glutamate: an update on their pharmacological involvement. Br J Pharmacol 150:5–17.

Benediktsson AM, Marrs GS, Tu JC, Worley PF, Rothstein JD, Bergles DE, Dailey ME. 2012. Neuronal activity regulates glutamate transporter dynamics in developing astrocytes. Glia 60:175–188.

Bergles DE, Tzingounis AV, Jahr CE. 2002. Comparison of coupled and uncoupled currents during glutamate uptake by GLT-1 transporters. J Neurosci 22:10153–10162.

Bordey A, Sontheimer H. 1997. Postnatal development of ionic currents in rat hippocampal astrocytes in situ. J Neurophysiol 78:461–477.

Brunne B, Zhao S, Derouiche A, Herz J, May P, Frotscher M, Bock HH. 2010. Origin, maturation, and astroglial transformation of secondary radial glial cells in the developing dentate gyrus. Glia 58:1553–1569.

Bushong EA, Martone ME, Ellisman MH. 2004. Maturation of astrocyte morphology and the establishment of astrocyte domains during postnatal hippocampal development. Int J Dev Neurosci 22:73–86.

Chaudhry FA, Lehre KP, van Lookeren Campagne M, Ottersen OP, Danbolt NC, Storm-Mathisen J. 1995. Glutamate transporters in glial plasma membranes: highly differentiated localizations revealed by quantitative ultrastructural immunocytochemistry. Neuron 15:711–720.

Cholet N, Pellerin L, Magistretti PJ, Hamel E. 2002. Similar perisynaptic glial localization for the Na+,K+-ATPase alpha 2 subunit and the glutamate transporters GLAST and GLT-1 in the rat somatosensory cortex. Cereb Cortex 12:515–525.

Cooper AJ, Lai JC. 1987. Cerebral ammonia metabolism in normal and hyperammonemic rats. Neurochem Pathol 6: 67–95.

Cooper AJ, McDonald JM, Gelbard AS, Gledhill RF, Duffy TE. 1979. The metabolic fate of 13N-labeled ammonia in rat brain. J Biol Chem 254:4982–4992.

Danbolt NC. 2001. Glutamate uptake. Prog Neurobiol 65:1–105.

Danbolt NC, Storm-Mathisen J, Kanner BI. 1992. An [Na^+ + K^+]coupled L-glutamate transporter purified from rat brain is located in glial cell processes. Neuroscience 51: 295–310.

Deitmer JW, Rose CR. 2010. Ion changes and signalling in perisynaptic glia. Brain Res Rev 63:113–129.

Derouiche A, Rauen T. 1995. Coincidence of L-glutamate/L-aspartate transporter (GLAST) and glutamine synthetase (GS) immunoreactions in retinal glia: evidence for coupling of GLAST and GS in transmitter clearance. J Neurosci Res 42:131–143.

Derouiche A, Anlauf E, Aumann G, Muhlstadt B, Lavialle M. 2002. Anatomical aspects of glia-synapse interaction: the perisynaptic glial sheath consists of a specialized astrocyte compartment. J Physiol Paris 96:177–182.

Freeman MR. 2010. Specification and morphogenesis of astrocytes. Science 330:774–778.

Fritschy JM. 2008. Is my antibody-staining specific? How to deal with pitfalls of immunohistochemistry. Eur J Neurosci 28:2365–2370.

Furness DN, Dehnes Y, Akhtar AQ, Rossi DJ, Hamann M, Grutle NJ, Gundersen V, Holmseth S, Lehre KP, Ullensvang K, Wojewodzic M, Zhou Y, Attwell D, Danbolt NC. 2008. A quantitative assessment of glutamate uptake into hippocampal synaptic terminals and astrocytes: new insights into a neuronal role for excitatory amino acid transporter 2 (EAAT2). Neuroscience 157:80–94.

Furuta A, Rothstein JD, Martin LJ. 1997. Glutamate transporter protein subtypes are expressed differentially during rat CNS development. J Neurosci 17:8363–8375.

Gilley JA, Kernie SG. 2011. Excitatory amino acid transporter 2 and excitatory amino acid transporter 1 negatively regulate calcium-dependent proliferation of hippocampal neural progenitor cells and are persistently upregulated after injury. Eur J Neurosci 34:1712–1723.

Hartfuss E, Galli R, Heins N, Gotz M. 2001. Characterization of CNS precursor subtypes and radial glia. Dev Biol 229: 15–30.

Haugeto O, Ullensvang K, Levy LM, Chaudhry FA, Honore T, Nielsen M, Lehre KP, Danbolt NC. 1996. Brain glutamate transporter proteins form homomultimers. J Biol Chem 271:27715–27722.

Hawkins RA, DeJoseph MR, Hawkins PA. 1995. Regional brain glutamate transport in rats at normal and raised concentrations of circulating glutamate. Cell Tissue Res 281: 207–214.

Helms HC, Madelung R, Waagepetersen HS, Nielsen CU, Brodin B. 2012. In vitro evidence for the brain glutamate efflux hypothesis: brain endothelial cells cocultured with astrocytes display a polarized brain-to-blood transport of glutamate. Glia 60:2523–2533.

Hughes EG, Maguire JL, McMinn MT, Scholz RE, Sutherland ML. 2004. Loss of glial fibrillary acidic protein results in decreased glutamate transport and inhibition of PKA-induced EAAT2 cell surface trafficking. Brain Res Mol Brain Res 124:114–123.

Ishikawa M, Yoshitomi T, Zorumski CF, Izumi Y. 2011. Downregulation of glutamine synthetase via GLAST suppression induces retinal axonal swelling in a rat ex vivo hydrostatic pressure model. Invest Ophthalmol Vis Sci 52:6604–6616.

Jungblut M, Tiveron MC, Barrai S, Abrahamsen B, Knöbel S, Pennartz S. Schmitz J, Perraut M, Pfrieger FW, Stoffel W, Cremer H, Bosio A. 2012. Isolation and characterization of living primary astroglial cells using the new GLAST-specific monoclonal antibody ACSA-1. GLIA 60:894–907

Kim JS, Kim J, Kim Y, Yang M, Jang H, Kang S, Kim JC, Kim SH, Shin T, Moon C. 2011. Differential patterns of nestin and glial fibrillary acidic protein expression in mouse hippocampus during postnatal development. J Vet Sci 12:1–6.

Kimoto H, Eto R, Abe M, Kato H, Araki T. 2009. Alterations of glial cells in the mouse hippocampus during postnatal development. Cell Mol Neurobiol 29:1181–1189.

Kudryashov IE, Onufriev MV, Kudryashova IV, Gulyaeva NV. 2001. Periods of postnatal maturation of hippocampus: synaptic modifications and neuronal disconnection. Brain Res 132:113–120.

Kugler P, Schleyer V. 2004. Developmental expression of glutamate transporters and glutamate dehydrogenase in astrocytes of the postnatal rat hippocampus. Hippocampus 14:975–985.

Langer J, Rose CR. 2009. Synaptically induced sodium signals in hippocampal astrocytes in situ. J Physiol 587:5859–5877.

Lee A, Pow DV. 2010. Astrocytes: Glutamate transport and alternate splicing of transporters. Int J Biochem Cell Biol 42:1901–1906.

Lehre KP, Danbolt NC. 1998. The number of glutamate transporter subtype molecules at glutamatergic synapses: chemical and stereological quantification in young adult rat brain. J Neurosci 18:8751–8757.

Lehre KP, Levy LM, Ottersen OP, Storm-Mathisen J, Danbolt NC. 1995. Differential expression of two glial glutamate transporters in the rat brain: quantitative and immunocytochemical observations. J Neurosci 15:1835–1853.

Lieth E, Barber AJ, Xu B, Dice C, Ratz MJ, Tanase D, Strother JM. 1998. Glial reactivity and impaired glutamate metabolism in short-term experimental diabetic retinopathy. Diabetes 47:815–820.

Liu X, Bolteus AJ, Balkin DM, Henschel O, Bordey A. 2006. GFAP-expressing cells in the postnatal subventricular zone display a unique glial phenotype intermediate between radial glia and astrocytes. Glia 54:394–410.

Magavi S, Friedmann D, Banks G, Stolfi A, Lois C. 2012. Coincident generation of pyramidal neurons and protoplasmic astrocytes in neocortical columns. J Neurosci 32:4762–4772.

Mathiisen TM, Lehre KP, Danbolt NC, Ottersen OP. 2010. The perivascular astroglial sheath provides a complete covering of the brain microvessels: an electron microscopic 3D reconstruction. Glia 58:1094–1103.

Matsugami TR, Tanemura K, Mieda M, Nakatomi R, Yamada K, Kondo T, Ogawa M, Obata K, Watanabe M, Hashikawa T, Tanaka K. 2006. From the cover: indispensability of the glutamate transporters GLAST and GLT1 to brain development. Proc Natl Acad Sci U S A 103:12161–12166.

Meyer L, Wildanger D, Medda R, Punge A, Rizzoli SO, Donnert G, Hell SW. 2008. Dual-color STED microscopy at 30-nm focal-plane resolution. Small 4:1095–1100.

Middeldorp J, Hol EM. 2011. GFAP in health and disease. Prog Neurobiol 93:421–443.

Minelli A, Barbaresi P, Reimer RJ, Edwards RH, Conti F. 2001. The glial glutamate transporter GLT-1 is localized both in the vicinity of and at distance from axon terminals in the rat cerebral cortex. Neuroscience 108:51–59.

Ming GL, Song H. 2005. Adult neurogenesis in the mammalian central nervous system. Ann Rev Neurosci 28:223–250.

Nakagawa T, Otsubo Y, Yatani Y, Shirakawa H, Kaneko S. 2008. Mechanisms of substrate transport-induced clustering of a glial glutamate transporter GLT-1 in astroglial-neuronal cultures. Eur J Neurosci 28:1719–1730.

Nixdorf-Bergweiler BE, Albrecht D, Heinemann U. 1994. Developmental changes in the number, size, and orientation of GFAP-positive cells in the CA1 region of rat hippocampus. Glia 12:180–195.

Nosyreva ED, Huber KM. 2005. Developmental switch in synaptic mechanisms of hippocampal metabotropic glutamate receptor-dependent long-term depression. J Neurosci 25:2992–3001.

Olabarria M, Noristani HN, Verkhratsky A, Rodriguez JJ. 2010. Concomitant astroglial atrophy and astrogliosis in a triple transgenic animal model of Alzheimer's disease. Glia 58:831–838.

Omrani A, Melone M, Bellesi M, Safiulina V, Aida T, Tanaka K, Cherubini E, Conti F. 2009. Up-regulation of GLT-1 severely impairs LTD at mossy fibre-CA3 synapses. J Physiol 587:4575–4588.

Peacey E, Miller CC, Dunlop J, Rattray M. 2009. The four major N- and C-terminal splice variants of the excitatory

amino acid transporter GLT-1 form cell surface homomeric and heteromeric assemblies. Mol Pharm 75:1062–1073.

Pekny M, Eliasson C, Siushansian R, Ding M, Dixon SJ, Pekna M, Wilson JX, Hamberger A. 1999. The impact of genetic removal of GFAP and/or vimentin on glutamine levels and transport of glucose and ascorbate in astrocytes. Neurochem Res 24:1357–1362.

Pfrieger FW. 2002. Role of glia in synapse development. Curr Opinion Neurobiol 12:486–490.

Pines G, Danbolt NC, Bjoras M, Zhang Y, Bendahan A, Eide L, Koepsell H, Storm-Mathisen J, Seeberg E, Kanner BI. 1992. Cloning and expression of a rat brain L-glutamate transporter. Nature 360:464–467.

Raponi E, Agenes F, Delphin C, Assard N, Baudier J, Legraverend C, Deloulme JC. 2007. S100B expression defines a state in which GFAP-expressing cells lose their neural stem cell potential and acquire a more mature developmental stage. Glia 55:165–177.

Reichenbach A, Derouiche A, Kirchhoff F. 2010. Morphology and dynamics of perisynaptic glia. Brain Res Rev 63:11–25.

Riol H, Fages C, Tardy M. 1992. Transcriptional regulation of glial fibrillary acidic protein (GFAP)-mRNA expression during postnatal development of mouse brain. J Neurosci Res 32:79–85.

Rodnight R, Goncalves CA, Wofchuk ST, Leal R. 1997. Control of the phosphorylation of the astrocyte marker glial fibrillary acidic protein (GFAP) in the immature rat hippocampus by glutamate and calcium ions: possible key factor in astrocytic plasticity. Braz J Med Biol Res 30:325–338.

Rothstein JD, Martin L, Levey AI, Dykes-Hoberg M, Jin L, Wu D, Nash N, Kuncl RW. 1994. Localization of neuronal and glial glutamate transporters. Neuron 13:713–725.

Schlag BD, Vondrasek JR, Munir M, Kalandadze A, Zelenaia OA, Rothstein JD, Robinson MB. 1998. Regulation of the glial Na+-dependent glutamate transporters by cyclic AMP analogs and neurons. Mol Pharmacol 53:355–369.

Schools GP, Zhou M, Kimelberg HK. 2006. Development of gap junctions in hippocampal astrocytes: evidence that whole cell electrophysiological phenotype is an intrinsic property of the individual cell. J Neurophysiol 96:1383–1392.

Seifert G, Huttmann K, Binder DK, Hartmann C, Wyczynski A, Neusch C, Steinhauser C. 2009. Analysis of astroglial K+ channel expression in the developing hippocampus reveals a predominant role of the Kir4.1 subunit. J Neurosci 29:7474–7488.

Shibata T, Yamada K, Watanabe M, Ikenaka K, Wada K, Tanaka K, Inoue Y. 1997. Glutamate transporter GLAST is expressed in the radial glia-astrocyte lineage of developing mouse spinal cord. J Neurosci 17:9212–9219.

Storck T, Schulte S, Hofmann K, Stoffel W. 1992. Structure, expression, and functional analysis of a Na(+)-dependent glutamate/aspartate transporter from rat brain. Proc Natl Acad Sci U S A 89:10955–10959.

Suarez I, Bodega G, Fernandez B. 2000. Modulation of glutamate transporters (GLAST, GLT-1 and EAAC1) in the rat cerebellum following portocaval anastomosis. Brain Res 859:293–302.

Sullivan SM, Lee A, Bjorkman ST, Miller SM, Sullivan RK, Poronnik P, Colditz PB, Pow DV. 2007a. Cytoskeletal anchoring of GLAST determines susceptibility to brain damage: an identified role for GFAP. J Biol Chem 282:29414–29423.

Sullivan SM, Macnab LT, Bjorkman ST, Colditz PB, Pow DV. 2007b. GLAST1b, the exon-9 skipping form of the glutamate-aspartate transporter EAAT1 is a sensitive marker of neuronal dysfunction in the hypoxic brain. Neuroscience 149:434–445.

Takasaki C, Okada R, Mitani A, Fukaya M, Yamasaki M, Fujihara Y, Shirakawa T, Tanaka K, Watanabe M. 2008. Glutamate transporters regulate lesion-induced plasticity in the developing somatosensory cortex. J Neurosci 28:4995–5006.

Takayasu Y, Iino M, Takatsuru Y, Tanaka K, Ozawa S. 2009. Functions of glutamate transporters in cerebellar Purkinje cell synapses. Acta Physiol 197:1–12.

Tanaka K, Watase K, Manabe T, Yamada K, Watanabe M, Takahashi K, Iwama H, Nishikawa T, Ichihara N, Kikuchi T, Okuyama S, Kawashima N, Hori S, Takimoto M, Wada K. 1997. Epilepsy and exacerbation of brain injury in mice lacking the glutamate transporter GLT-1. Science 276:1699–1702.

Ullensvang K, Lehre KP, Storm-Mathisen J, Danbolt NC. 1997. Differential developmental expression of the two rat brain glutamate transporter proteins GLAST and GLT. Eur J Neurosci 9:1646–1655.

Ullian EM, Christopherson KS, Barres BA. 2004. Role for glia in synaptogenesis. Glia 47:209–216.

Vallejo-Illarramendi A, Domercq M, Matute C. 2005. A novel alternative splicing form of excitatory amino acid transporter 1 is a negative regulator of glutamate uptake. J Neurochem 95:341–348.

Verbich D, Prenosil GA, Chang PK, Murai KK, McKinney RA. 2012. Glial glutamate transport modulates dendritic spine head protrusions in the hippocampus. Glia 60:1067–1077.

Vina JR, DeJoseph MR, Hawkins PA, Hawkins RA. 1997. Penetration of glutamate into brain of 7-day-old rats. Metab Brain Dis 12:219–227.

Watase K, Hashimoto K, Kano M, Yamada K, Watanabe M, Inoue Y, Okuyama S, Sakagawa T, Ogawa S, Kawashima N, Hori S, Takimoto M, Wada K, Tanaka K. 1998. Motor discoordination and increased susceptibility to cerebellar injury in GLAST mutant mice. Eur J Neurosci 10:976–988.

Weir MD, Thomas DG. 1984. Effect of dexamethasone on glutamine synthetase and glial fibrillary acidic protein in normal and transformed astrocytes. Clin Neuropharm 7:303–306.

Willig KI, Kellner RR, Medda R, Hein B, Jakobs S, Hell SW. 2006. Nanoscale resolution in GFP-based microscopy. Nat Methods 3:721–723.

Wu Y, Zhang AQ, Yew DT. 2005. Age related changes of various markers of astrocytes in senescence-accelerated mice hippocampus. Neurochem Int 46:565–574.

Yang Y, Gozen O, Watkins A, Lorenzini I, Lepore A, Gao Y, Vidensky S, Brennan J, Poulsen D, Won Park J, Li Jeon N, Robinson MB, Rothstein JD. 2009. Presynaptic regulation of astroglial excitatory neurotransmitter transporter GLT1. Neuron 61:880–894.

Zhou J, Sutherland ML. 2004. Glutamate transporter cluster formation in astrocytic processes regulates glutamate uptake activity. J Neurosci 24:6301–6306.

Zhou M, Schools GP, Kimelberg HK. 2006. Development of GLAST(+) astrocytes and NG2(+) glia in rat hippocampus CA1: mature astrocytes are electrophysiologically passive. J Neurophysiol 95:134–143.

Zhu X, Bergles DE, Nishiyama A. 2008. NG2 cells generate both oligodendrocytes and gray matter astrocytes. Development 135:145–157.